PONTIFICIA UNIVERSIDAD CATOLICA DE CHILE
ESCUELA DE INGENIERIA

THERMODYNAMIC PROPERTIES OF CO_2 DURING CONTROLLED DECOMPRESSION OF SUPERCRITICAL EXTRACTION VESSELS

EDUARDO ADOLFO RICHTER DIETHELM

Thesis submitted to the Office of Research and Graduate Studies in partial fulfilment of the requirements for the Degree of Master of Science in Engineering.

Advisor
JOSÉ MANUEL DEL VALLE

Santiago de Chile, (March, 2015)

PONTIFICIA UNIVERSIDAD CATOLICA DE CHILE
ESCUELA DE INGENIERIA

THERMODYNAMIC PROPERTIES OF CO_2 DURING CONTROLLED DECOMPRESSION OF SUPERCRITICAL EXTRACTION VESSELS

EDUARDO ADOLFO RICHTER DIETHELM

Members of the Committee:

JOSÉ MANUEL DEL VALLE

MAGDALENA WALCZAK

GONZALO NÚÑEZ

JOSÉ FRANCISCO MUÑOZ

Thesis submitted to the Office of Research and Graduate Studies in partial fulfilment of the requirements for the Degree of Master of Science in Engineering

Santiago de Chile, (March, 2015)

To my parents, wife, and daughters.

ACKNOLEDGEMENTS

To Granasur S.A. for kindly providing us the samples of oilseeds for our studies in supercritical extraction and heat transfer during blowdown of supercritical vessels. To the *Comisión Nacional de Investigación Científica y Tecnológica* CONICYT for financing the Fondecyt project number 1120827. To Professor José Francisco Muñoz for asking the basic questions that made me review the fundaments of my work. To professor Magdalena Walczak and Dr. Manuela Covaciou for working with me in the generation of the metallic foams. To the present and former students and investigators of LEMaB, for helping and commenting my work. To Philip Jaeger for designing the special measuring instruments. To Professor Gonzalo Núñez, for his assistance in the experiments. And finally to professor José Manuel del Valle for his advises and for introducing me in the supercritical fluids.

Vivat Academia,
vivant professores.
Vivat membrum quodlibet,
vivant membra quaelibet,
semper sint in flore.

GENERAL INDEX

Page.

LIST OF TABLES

Page

LIST OF FIGURES

Page

RESUMEN

Descompresiones muy rápidas de recipientes de alta presión disminuyen la temperatura de sus paredes por debajo de -10 ºC, volviéndose quebradizos. Por ello, la descompresión podría limitar el tiempo de extracción en plantas industriales de extracción con CO_2 supercrítico (aumentando los costos de producción). Este trabajo estudió descompresiones de CO_2 inicialmente a 30 MPa en un recipiente de 3.96 L venteado controladamente a través de una válvula de aguja. Esta apertura controlada evitó que el CO_2 formara una mezcla líquido-gas en el recipiente. Las caídas de presión fueron rápidas al comienzo y al final de las descompresiones, y comparativamente lentas en el intervalo entre 10–15 MPa, antes que el CO_2 cruzara la línea pseudocrítica. La temperatura cayó al comienzo de las descompresiones, se mantuvieron estables en el intervalo intermedio y aumentaron al final. El tiempo de descompresión fue inversamente proporcional a la apertura de la válvula, y fue menor partiendo a 60 que a 50 ºC. La caída de temperatura fue proporcional a la apertura de la válvula. Al empacar semillas de rosa mosqueta o frambuesa prensadas o prensadas y peletizadas previamente extraídas, el tiempo de descompresión dependió de la porosidad total del sustrato. Observándose flujo ahogado en el asiento de la válvula, el flujo evacuado depende de su apertura. Para estimar los cambios en la energía interna del CO_2 en el recipiente, se necesita incorporar al balance de energía transiente tanto el calor provisto por el fluido de servicio, como el calor cedido por la pared del recipiente y el sustrato cargado. Los resultados de este trabajo sirven para validar un modelo que simule descompresiones de extractores industriales en función de su tamaño y forma, las condiciones de extracción, y el sustrato empacado. Los tiempos de descompresión predichos restringirían los tiempos de reacondicionamiento de extractores en estudios de minimización de costos de producción.

Palabras Claves: Flujo ahogado; Descompresión; Recipiente de alta presión; Transferencia de calor; Lecho empacado; CO_2 supercrítico.

ABSTRACT

Fast decompressions of extraction vessels reduce the temperature of their walls below the −10 ºC limit which turns them brittle. Therefore, decompression of large vessels operating at high pressure may set a lower limit of extraction time in industrial multi-vessel supercritical CO_2 extraction plants (thus negatively influencing production cost).

This work studied decompression of CO_2 initially at 30 MPa in a 3.96 L vessel vented through a partially opened needle valve. Slow CO_2 venting avoided a two-phase (liquid-gas) mixture in the vessel. Pressure drop was abrupt at the beginning and the end of decompressions, and comparatively smoother within the 10–15 MPa interval, before CO_2 crossed the pseudocritical line. Temperature dropped at the beginning of decompressions, remained comparatively constant in an intermediate period, and increased at the end. Decompression time was inversely proportional to valve opening, and was shorter when starting at 60 compared to 50 ºC. The initial drop in temperature was proportional to valve opening. When packing pretreated (either pressed or pressed/pelletized) and extracted rosehip or raspberry seeds depressurization time was proportional to the porosity of the packed bed and independent on other properties of the substrate. Being flow through the needle valve choked, venting rate was determined by its opening and the physical properties of CO_2 in the vessel. To estimate the changes in internal energy of the CO_2 in the vessel that define vessel wall's temperature, the heat provided by the service fluid, the heat yield by the material of the high-pressure vessel, and the heat yield by the substrate charge need to be incorporated to the transient heat balance. The results obtained in this work can be used to validate a model of the depressurization process that could simulate decompressions of industrial vessels as a function of their size and shape, the extraction conditions, and the packed substrate. Predicted decompression times would restrict the setup times of industrial vessels in studies of minimization of production cost.

Key words: Chocked flow; Decompression; Extraction vessel; Heat transfer; Packed bed; Supercritical CO_2.

1 INTRODUCTION

Supercritical CO_2 has a great potential as an extraction solvent, but the profitability of the industrial process is still questioned (del Valle 2014). Because the solvent power of supercritical CO_2 is easily tuned by changing system pressure and temperature, a good tradeoff between yield and selectivity is obtained (Brunner 2005), but production cost can be high. Changing operational conditions with the purpose of lowering production cost (*e.g.*, decreasing particle size, increasing solvent flow rate, increasing extraction pressure) lower extraction time as well (del Valle 2014; Núñez & del Valle 2014). On the other hand, increasing the number of extraction vessels of the plant with the same purpose of lowering production cost may decrease setup time (the time when the extraction vessel in an industrial plant is out of the solvent cycle), even if the optimal extraction time increases (del Valle 2014; Núñez & del Valle 2014). Finally, because of economies of scale, production cost also decrease when increasing the size of extraction vessels (del Valle 2014; Núñez & del Valle 2014). The aforementioned alternatives reduce the available time for setup, but this could be particularly slow for large extraction vessels operating at high pressure, exactly the conditions recommended to reduce production cost (del Valle 2014).

Decompressing extraction vessels may limit setup time because of the limited heat transfer rate in these systems. The setup of an extractor consists in recovering/venting the CO_2 remaining in the vessel after an extraction cycle, replacing the exhausted substrate with fresh one, and filling the vessel with CO_2 up to the required extraction pressure (Eggers & Jaeger 2003). Temperature descends along with pressure during decompression; temperature drop due to the Joule-Thomson effect in adiabatic decompressions (Stanley 1998; Reverchon & Osséo 1994) may even reach a level where dry ice is formed. Although heat is transferred from the vessel's walls and the substrate to the expanding CO_2, heat transfer may be limited and temperature may drop to a very low level if depressurization is fast (Eggers & Green 1990; Green & Eggers 1991). Depressurization of industrial vessels should be as fast as possible under the restriction of preventing low temperatures below -10 ºC to prevent their stainless steel walls

from becoming brittle (Smallman & Ngan 2007). A computational model could determine a minimum decompression time. This model should be based in momentum and heat balance and transport equations, and include the size and shape of the extraction vessel, the initial conditions of CO_2, and the properties of extracted substrate as parameters.

The mechanisms of heat transfer for the controlled decompression of supercritical CO_2 from an extraction vessel have been rarely studied. Previous works in decompression were done concerning the safety of pressure vessels (Eggers & Green 1990; Gebbeken & Eggers 1996; Zhang et al. 2014). Because the most dangerous case is when the vessel is full of fluid, the influence of the packed bed on pressure and temperature changes was barely studied. Eggers and Green (1990) described the effect of the packed bed on decompressions, but they only guessed reasons of changes as compared to a vessel full of fluid, and did not relate these changes to the properties of the substrate. Other authors studied heat transfer from a packed bed to a flowing gas (Sheikholeslami & Watkinson 1998; Laguerre et al. 2006). Finally, heat transfer to supercritical fluids is faster than to gases or liquids (Pioro & Duffey 2007), with special correlations for Nusselt numbers in pipelines or packed beds as function of Reynolds, Grasshof, and Prandlt numbers being proposed (Bae 2011; S. M. Liao & Zhao 2002; Guardo et al. 2006). Unfortunately, these separate studies were made in different fields and applications and the interaction between all factors is not clear. Therefore, the merged model to calculate heat transfer during the venting of a vessel with an extracted substrate mentioned at the end of the previous paragraph cannot be validated without an experimental study of the process.

1.1 Hypothesis and objectives

The purpose of this work was to validate a mathematical model that optimizes decompression time of industrial vessels. Experiments at pilot scale should check mass and energy balance, and heat transfer in the system. Also, experiments should provide curves of pressure and temperature *versus* decompression time for validation. The

working hypothesis was that the substrate, the initial pressure and temperature, and the venting rate will affect the venting time, the lowest temperature at the wall of the vessel, and the temperature profiles within the packed bed.

This thesis is organized as follows: Section 2, Literature Survey, describes the state of arts introducing the reader to supercritical fluid extraction and its processes, and description of existing work in heat transfer and packed bed characterization. Sections 3 to 5 are Materials and Methods, Results, and Discussion, as they were written in the article published in The Journal of Supercritical Fluids by Richter *et. al* (2015). Finally, Section 6 collects the principal conclusions of this research and poses the state of the future work on the topic.

2 LITERATURE REVIEW

The following section is structured as follows. Subsection 2.1 introduces the reader to supercritical fluids, their advantages as a solvent for separation processes, and the advances in industrial applications of supercritical fluid extraction. Subsection 2.2 briefly reviews the state of art on heat transfer that could apply to the studied problem, including heat transfer in supercritical fluids, and heat transfer due to natural convection on plates and within enclosures. Finally, Subsection 2.3 covers packed beds; reviewing the properties that describe them, and heat transfer in them.

2.1 Supercritical fluid extraction and its applications to industrial processes

A Supercritical (Sc) Fluid (ScF) is defined as a substance whose pressure and temperature are above its corresponding supercritical conditions. Under these conditions, no condensation takes place either under an isotermic compression or an isobaric cooling. Thermophysical and transport properties of supercritical fluids can vary strongly with changes in pressure and temperature. ScFs have two distinguishable regions, with gas-like properties and liquid-like properties, respectively. The boundary between both regions is defined as the pseudocritical line; which coincides with the local maxima of the specific heat (Pioro et al. 2011). This pseudocritical line nears the isochoric line that passes through the critical point. For the specific case of carbon dioxide (CO_2), the critical point is at 30.7 ºC and 7.3 MPa. Saturation and solidification lines, the critical point, the pseudocritical line and the supercritical region, and densities and specific enthalpies of the CO_2 are shown in a *P versus T* diagram in Figure 2-1.

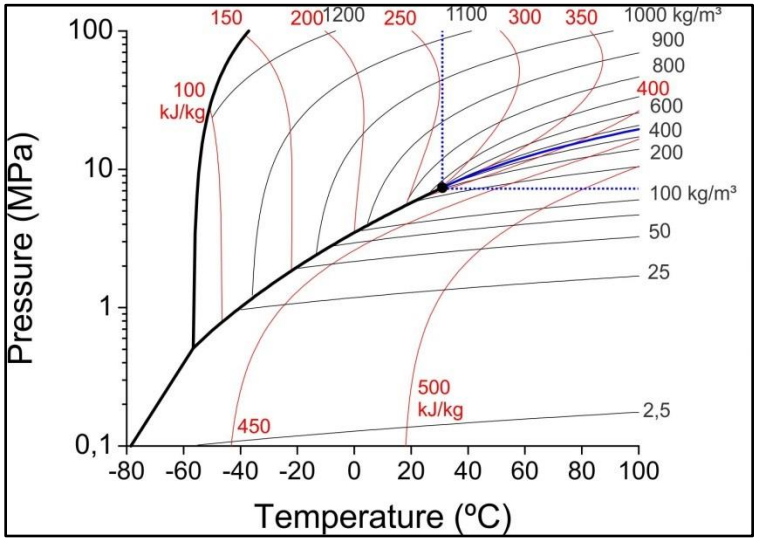

Figure 2-1. Pressure *versus* Temperature diagram for CO_2 (Lemmon et al. 2007). (—) Saturation or solidification line; (•) critical point; (—) pseudocritical line; (·····) supercritical region; (—) isochoric line; and, (—) adiabatic line.

Sc CO_2 has many advantages to be used as a solvent for industrial extraction processes. Solubility of interest compounds in Sc CO_2 depends sharply on its temperature and density (or pressure) (del Valle & Aguilera 1988). Thus, Sc CO_2 is a tunable and selective solvent: tunable because changing from a high to a low solubility (*e.g.*, for separation of solutes from the solvent) is achieved changing pressure; selective because conditions can be tuned to solubilize some compounds and not others (*e.g.*, for fraction). Other advantages are its harmlessness, low polarity, low corrosivity or reactivity, and its relatively low price (del Valle & Aguilera 1988). In conclusion, Sc CO_2 is a good alternative to organic solvents for separation of natural compounds.

The first industrial application of Sc CO_2 in the '70s was decaffeination of coffee beans; nowadays it is used for a wide number of processes in the food industry. Some of the most common industrial applications of ScF Extraction (ScFE) in the industry are (1) extraction of flavourings (*e.g.*, essential oils) from herbs and spices; (2) extraction of hops for brewing industry, (3)extraction and refining oils and fats; (4) extraction of natural colorants and antioxidants (*e.g.*, lycopene, astaxantin); (5) removal of undesirable compounds from a valuable matrix (*e.g.*, caffeine, nicotine, or cholesterol);

and, (6) fractioning of solutes from aqueous mixtures (*e.g.* ethanol, natural flavour) (Brunner 2005; del Valle & Aguilera 1999).

Industrially, Sc CO_2 is used mainly in two different extraction processes: extracting a solid material as shown in Figure 2-2A or fractioning a liquid mixture as shown in Figure 2-2B. Both processes present a solvent cycle consisting mainly of pressurizing CO_2 stored in a buffer tank, and heating or cooling it to the extraction conditions, contacting it with the mixture or material, decompressing and heating it to separate the solutes, and cooling it to store it as saturated liquid. Fractioning is performed in packed columns to maximize the mass transfer area and are done in a continuous process. Extraction of solid materials is perforce a batch process; with a setup time to replace depleted substrate by fresh one. Designs of an extraction plant that continuously charges fresh material into the high-pressure vessel and removes depleted ones (Eggers 1996) have not been implemented at industrial scale to replace the traditional batch process. To emulate a counter current arrangement, one extractor is in setup, while the rest are in the solvent cycle.

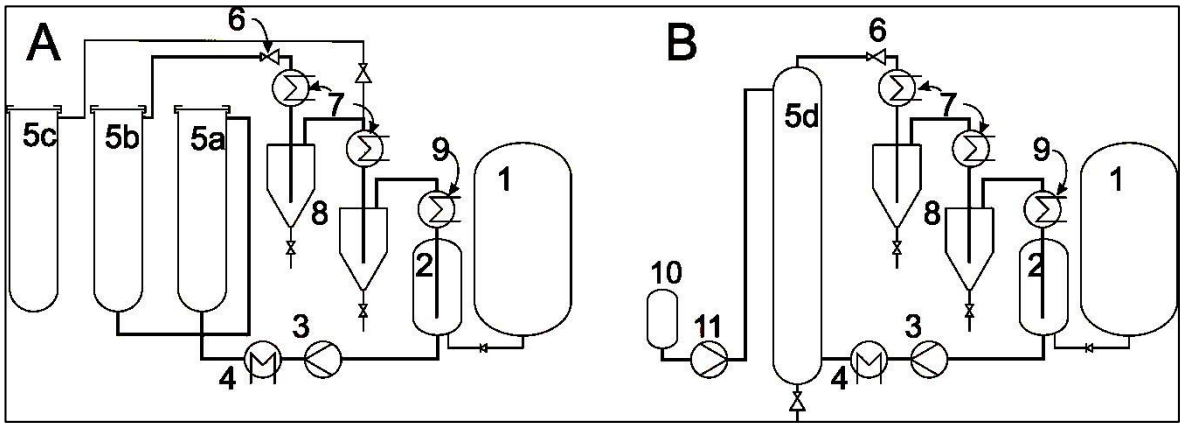

Figure 2-2. (A) Diagram of a supercritical fluid extraction plant for solid extraction; (B) Diagram of a supercritical fluid extraction plant for liquid fractioning. Legend: (1) CO_2 storing tank; (2) solvent buffer tank; (3) solvent pump; (4) heat exchanger; (5a–5c) extractors; (5d) column; (6) back-pressure regulator (BPR); (7) heating coils; (8) separation cyclons; (9) condenser; (10) Substrate tank; (11) substrate pump

2.2 Packed beds and their physical properties.

A packed bed is a vessel or recipient filled with small particles. They are widely used in chemical engineering applications because they have a large specific surface that enhances heat and mass transfer in a small volume (Thadani & Peebles 1966). Therefore, substrates for ScFE are almost always charged in the extraction vessels as packed beds with particles as small as possible. The properties of particles and packed beds used in the present work are described in the following subsections.

2.2.1 Particle size and shape

Particle size (and its distribution) and particle shape are the most important parameters to characterize a sample of particles and determine characteristics of packed beds they conform. For particles of irregular shape there is no unique measure to describe particle size, opposite to regular particles such as spheres or cubes. An equivalent diameter D_p is therefore defined as the diameter of a spherical particle that shares a given property with the measured particle (McCabe & Smith 1968). It can be the distance between two parallel tangent lines (*e.g.*, for sieving), the longest dimension of the particle, same volume, same terminal velocity (*e.g.*, for sedimentation), etc. For heat and mass transfer processes the relevant particle size is the diameter of equivalent specific surface (or Sauter diameter). This diameter assures that for a given volume of particles (*i.e.*, mass of particles if particle density is known), the same specific surface for transport phenomena will be available than in a packed bed formed of spheres of the equivalent diameter. However its usefulness, this diameter is hard to determine unless assumptions on the particle's shape are done. The shape of irregular particles is even more difficult to determine, and either numerical or verbal descriptors are used. One useful descriptor is shape factor λ, which relates the ratio between the volume and the surface of a particle V_p and S_p, respectively with its diameter, as shown in Eq. (1) (McCabe & Smith 1968):

$$\frac{V_p}{S_p} = \frac{D_p}{6\lambda} \tag{1}$$

2.2.2 Density

For a volume of particles, different densities can be defined, depending on the volume used in the definition of density. As described by Maguet *et al.* (2005), three different volumes can be distinguished for a bed of porous particles: volume occupied by solid material V_s, volume occupied by particles V_p (*i.e.* volume of the solid plus volume of pores within the particle), and bulk volume V_g (*i.e.* volume of the particles plus interparticle space volume). The difference between these three volumes is shown in Figure 2-3. Solid density (ρ_s), particle density (ρ_p) and bulk density (ρ_g) are the relationships between the packed mass and the corresponding volumes.

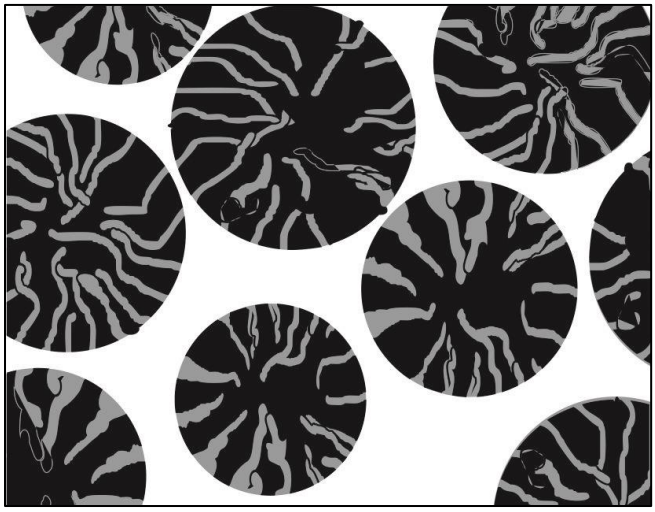

Figure 2-3: Schematic cut of a packed bed showing volumes of the solid (■), the pores (▭) and the interparticle space (□)

2.2.3 Interparticle, intraparticle, and total porosity.

Porosity is a property of two-phase materials, defined as the volume fraction that could be occupied by a displacing fluid. Intraparticle porosity ε_i refers as the fraction of the particle volume corresponding to intraparticle pores, or the compliment to the fraction of solids within the particles. Interparticle porosity ε_e refers to the fraction of the bed volume not occupied by particle. Total porosity ε_t refers to the fraction of the bulk volume not occupied by solid material. Porosities can be calculated as relationships

between densities as well (Mauguet et al. 2005). Assuming that the particle mass equals the particle volume (*i.e.,* the fluid in the intraparticle pores has no measurable mass), intraparticle porosity Eq. (2), and interparticle porosity Eq. (3) are calculated as a function of densities, while total porosity Eq. (4) is calculated as a weighting between interparticle and intraparticle porosity.

$$\varepsilon_i = 1 - \frac{V_s}{V_p} = 1 - \frac{m_s / \rho_s}{m_p / \rho_p} = 1 - \frac{\rho_p}{\rho_s}, \tag{2}$$

$$\varepsilon_e = 1 - \frac{V_p}{V_g} = 1 - \frac{m_p / \rho_p}{V_g} = 1 - \frac{\rho_g}{\rho_p}, \text{ and} \tag{3}$$

$$\varepsilon_t = 1 - \frac{V_s}{V_g} = \frac{V_g - V_p + V_p - V_s}{V_g} = \varepsilon_e + \frac{V_p - V_s}{\frac{V_g * V_p}{V_p}} = \varepsilon_e + (1 - \varepsilon_e) * \varepsilon_i . \tag{4}$$

Bed porosity is determined by the size and shape of the packed particles. For regular shapes like spheres or cylinders with an equal height and diameter, the mean porosity was correlated to the ratio of the diameter of the particles and the diameter of the cylindrical vessel. Generally, bed porosity reaches a constant value when this ratio is below 0.1. For a same size, packed beds of spheres have a higher porosity than those of cylinders (Benyahia & O'Neill 2005; Dixon 1988). The porosities of packed beds of spheres and cylinders are plotted versus standardized particle size in Figure 2-4. For small particles, in both models cylinders have less bed porosity than spheres for the same size. In both models the asymptotic porosity (*i.e.,* the bed porosity for particles packed in a vessel at least 10 times larger than the particle size) of spheres and cylinders are around 0.39 and 0.37 respectively. Also, both models predict a maximum porosity around a relative particle size of 0.6. The effect of aspect ratio H/d_p of cylinders on its asymptotic porosity was studied by Benyahia & O'Neill (2005), but the variation was within the standard error of the correlation.

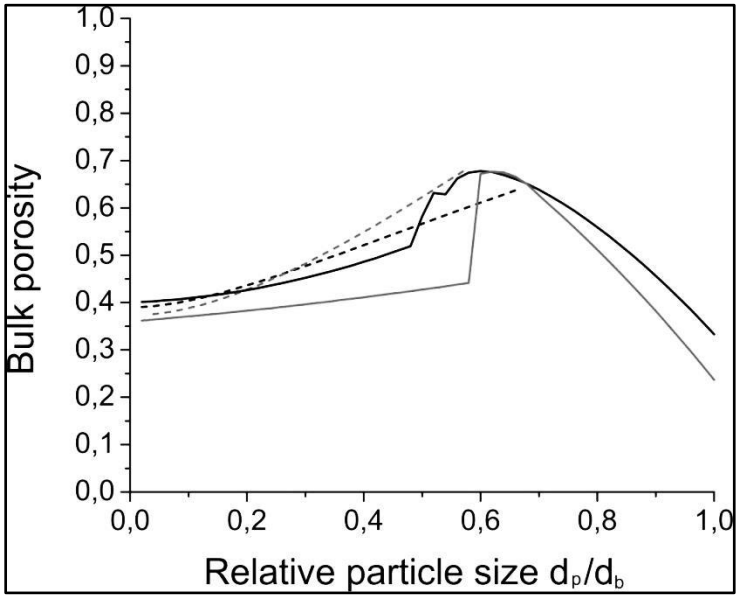

Figure 2-4 Comparisson of the porosities of spheres (black) and solid cylinders (grey) as a function of the relative particle size (*i.e.*, the relationship between the particle size and the diameter of the containing vessel as proposed by Dixon (1988) (solid lines) and Benyahia & O'neill (2005) (dashed lines)

In fact, local bed porosity near the wall of the vessel oscillates as function of the particle size. Also, for similar particle sizes, the shape of particles affects the bulk porosity, where less spherical particles give rise to beds of lower porosity (Thadani & Peebles 1966; Montillet & Coq 2001).

2.3 Heat transfer during decompression of high-pressure vessels

Heat transfer in fluids has been postulated as the exchange of kinetic energy between molecules vibrating with different internal energies (Kakaç & Yener 1987). For convection, this exchange is improved due to the movement of the fluid, which mixes molecules with different internal energies. When a fluid is near a surface at a different temperature, molecules near the surface will exchange energy and will be carried away by the motion of the fluid. Therefore, a thin boundary layer will be formed, where the temperature lies between the temperatures of the fluid and the solid surface. The heat flux Q/A, where Q is the heat transferred, and A is the contact surface between the solid and the fluid, is proportional to this temperature difference (Kakaç & Yener 1987). The dimensionless Nusselt number Nu relates the heat transfer between a surface and a fluid

due to convection (expressed as a convective heat transfer coefficient *h*), compared to the heat transferred through a characteristic dimension *L* only due to the thermal conductivity of the fluid *k* (Pletcher 1987). Thus, it can be written as Eq. (5):

$$Nu = \frac{hL}{k}. \tag{5}$$

The most common approach to estimate a heat transfer coefficient is to correlate *Nu* with other dimensionless numbers. None of the sources reviewed for this work treated the problem of transient heat transfer of a SCF in an enclosure. Therefore, stationary heat transfer in SCF, heat transfer of normal fluids under natural convection, heat transfer in enclosures, and heat transfer in packed beds are reviewed separately in Subsections 2.3.1, 2.3.2, 2.2.3, and 2.3.4, respectively.

2.3.1 Heat transfer in supercritical fluids

Heat transfer in ScF has been studied lately for their use in power plants. All works coincide that heat transfer in ScF is faster than in liquids or gases. The majority of the studies are related to convective heat transfer in natural or forced flow through pipes or annular sections; a few are reviewed next. To the best of the author's knowledge, the only work on convection from particles of a packed bed in a supercritical fluid was done by Guardo *et al.* (2006) to model fixed bed catalytic reactors, and is reviewed at the end of this subsection.

All correlations found for Nusselt number of supercritical fluids flowing in pipes are modifications of the Dittus-Boelter equation adjusted to fit the enhancement of heat transfer in supercritical fluids. They can be resumed in Eq. (6):

$$Nu = A\left(Re\right)^{B}\left(Pr\right)^{C}\left(\frac{\rho_w}{\rho_b}\right)^{D}\left(\frac{c_{p_b}}{c_{pw}}\right)^{E} f\left(\frac{Gr}{Re^{\alpha}}\right), \tag{6}$$

where $Re\left(=\frac{v\rho L}{\mu}\right)$, and $Pr\left(=\frac{c_p\mu}{k}\right)$ are the dimensionless Reynolds number and Prandtl number, respectively (ρ, μ, c_p, and k are the density, viscosity, specific heat and thermal conductivity of the fluid, while v is the velocity of the fluid and L is the pipe's

diameter) . A – E are best-fitting parameters, where D and E quantify the enhancement of heat transfer in ScFs due to the sharp change of density and specific heat as temperature changes. Finally, $f\left(\frac{Gr}{Re^{\alpha}}\right)$ correct the heat transfer coefficient due to the high buoyancy, as a relationship between the dimensionless Grashof number and the Reynolds number. The Grashof number (Eq. 7)

$$Gr = \frac{g\beta L^3 \left(T_w - T_\infty\right)\rho^2}{\mu^2} \tag{7}$$

compares the buoyance to the viscous force opposing buoyancy, where g is the gravitational acceleration, β ($=\frac{1}{V}\frac{dV}{dT}$) is the volumetric thermal expansion coefficient.

The parameters A to E are shown in Table 2-1. Each parameter was not necessarily in the same order than in correlations for normal fluids; either a higher proportionality coefficient or a higher dependence on Prandtl number was observed, factors that quantify the enhancement of heat transfer near to the supercritical region.

Table 2-1. Coefficients for the correlation for Nusselt dimensionless number as proposed for several authors, following the general form: $Nu = A\left(Re\right)^{B}\left(Pr\right)^{C}\left(\frac{\rho_w}{\rho_b}\right)^{D}\left(\frac{c_{p_b}}{c_{pw}}\right)^{E}$

Study	Type of flow	A	B	C	D	E
(S.M. Liao & Zhao 2002b)	Horizontal	0.128	0.8	0.3-0.4*	0.842	0,384
(S.M. Liao & Zhao 2002a)	Ascendant	0.354	0.8	0.3-0.4*	1.297	0,296
	Descendant	0.643	0.8	0.3-0.4*	2.154	0,751
(Bae 2011)	–	0.021	0.8	0.55	–	0.35

*The value of C may vary from 0.3 to 0.4 depending if the fluid is being cooled or heated.

If the forced flow is not high enough, then buoyancy will be significant as well. To consider this effect, a buoyancy correction factor will be applied to the forced convection coefficient, which will be a function of Grashof number. Since the Grashof number of supercritical fluids is normally high, buoyancy is relevant even at high Reynolds numbers. The corrections for buoyancy are listed in Table 2-2.

Table 2-2. Buoyancy correction $f\left(\frac{Gr}{Re^{\alpha}}\right)$ for Nusselt correlations

Study	Type of flow	$f\left(\frac{Gr}{Re^{\alpha}}\right)$
(S. M. Liao & Zhao 2002b)	Horizontal	$\left(\frac{Gr}{Re^{2}}\right)^{0,203}$
(S. M. Liao & Zhao 2002a)	Ascendant	$\left(\frac{Gr}{Re^{2,7}}\right)^{0,157}$
	Descendant	$\left(\frac{Gr}{Re^{2,7}}\right)^{0,186}$
(Bae 2011)	Ascendant	$\begin{cases}\left(1-8000\left(\frac{Gr}{Re^{2,7}}\right)\right)^{0,5}, if\left(\frac{Gr}{Re^{2,7}}\right)\le 10^{4} \\ 15\left(\frac{Gr}{Re^{2,7}}\right)^{0,38}, if\left(\frac{Gr}{Re^{2,7}}\right)>10^{4}\end{cases}$
	Descendant	$\left(1+30.000\left(\frac{Gr}{Re^{2,7}}\right)\right)^{0,3}$

Guardo *et. al.* (2006) analysed particle-to-fluid heat transfer in a packed bed using Computational Fluid Dynamics to model fixed bed reactors. They created an arrangement of 44 spheres in a cylinder, overlapping 5% of the particles to avoid convergence problems and to have real contact points. They assumed a constant temperature within the particles and a flow regimen ranging from $0,33<Re<3300$.

They identified that heat transfer was due to combined forced and natural convection in laminar flow. They proposed a mixed correlation for the dimensionless Nusselt

number, valid for 9 <Re <96; 2.2 <Pr <3.3, and 1×10^{8} <Gr <4×10^{10}, which is the addition of natural Nusselt (Eq. 8) and the forced Nusselt (Eq 9):

$$Nu_{\text{natural}} = Nu_0 + 0.001\left(GrPr\right)^{0.33} Pr^{0.244} \text{ , and} \tag{8}$$

$$Nu_{\text{forced}} = 0.269 Re^{0.88} Pr^{0.3}, \tag{9}$$

where Nu_0 as a reference Nusselt number (*e.g.* Nu_0=2). Although this equation was near to the application studied in this work, it only includes convection from the particle to the fluid in the interparticle space, and does not take in account heat propagation from the walls of the vessel to the bulk of the packed bed.

2.3.2 Heat transfer due to natural convection in normal fluids

Natural convection is the mechanism in which convective flow is solely produced by density gradients within the fluid due to temperature (or concentration) gradients. Buoyant forces (*i.e.*, the difference in the gravity attraction of the more dense fluid) will cause a flow around a body of different temperature than the surrounding fluid. The flow pattern of the fluid will depend on the temperature difference and the decrease in density as a result of an increase in temperature, rising if the fluid takes heat, and sinking if the fluid releases heat. Because it is observed in many natural and artificial processes, natural convection is widely treated in books (Kaviany 1994; Kakaç et al. 1987).

Since the driving force for natural convection is buoyancy, the Grashof number is of mayor relevance. Together with the Prandtl number, the Grashof number is used to correlate the Nusselt number for different geometries, being the vertical plate the most commonly studied. Particularly the correlation proposed by Ede and reviewed by Kaviany (1994) is frequently used (Eq. 10):

$$Nu = \frac{3}{4}\left(\frac{2Pr}{5\left(1+2\sqrt{Pr}+2Pr\right)}\right)^{1/4}\left(GrPr\right)^{1/4} \tag{10}$$

The correlation for a vertical plate could be used for other vertical geometries if the boundary layer of buoyant flow is small enough in comparison to the curvature of the

vertical shape. Boundary layer x_l can be calculated as a function of the height of the plate L, as proposed by Gebhart *et al.*, as reviewed by Kaviany (1994) in Eq. (11):

$$x_{bl} = \frac{3.93L\left(Pr + \frac{20}{21}\right)^{1/4}}{\sqrt{(\sqrt{Gr}Pr)}}, \tag{11}$$

2.3.3 Natural convection in enclosures

An enclosure is defined as a space with solid boundaries filled with a fluid. Heat transfer within an enclosure occurs due to buoyancy induced at the boundaries at a different temperature. Natural convection in enclosures was studied in a variety of applications, including furnaces and ovens, heat losses in solar collectors and insulating double windows, and cooling of electronic devices. These subjects are reviewed in books covering convective heat transfer (Yang 1987). The more correct approach is to model the streamlines using theoretical or numerical methods, which is beyond the scope of this work. However, it is anticipated that general descriptive correlations for the average Nusselt number in an enclosure could be a function of Rayleigh and Prandtl numbers, and geometrical factors such as aspect ratio height to width of the enclosure.

An asymptotic analysis can predict whether heat transfer in an enclosure is limited by conduction or by convection in a boundary layer. If the Rayleigh number is very small, then the fluid could be considered as stagnant, and heat will be transferred by conduction. On the other hand, if the Rayleigh number is sufficiently high, thin boundary layers will be formed along the transferring walls, whereas the core of the fluid will remain relatively stagnant.

Correlations for Nusselt numbers in enclosures have been estimated either by experimental measurements, or by numerical calculations. These correlations are classified into two-dimensional (*e.g.*, rectangles or circles) or three-dimensional (*e.g.*, cylinders, spheres, cubes). The more relevant functions for our work are vertical cylinders or vertical rectangles (*i.e.* an axial cut of our cylinder). Many of the correlations reviewed by Yang (1987) were of the form $Nu = aRa^b$, where a and b are

best-fitting parameters, that depend on the size and shape of the enclosure, and the range of the Prandtl and Rayleigh numbers. The values of the parameters varies between 0.05 <*a* <1.3, and 0.23 <b <0.33, and correlations were valid for a wide range of Prandtl and Rayleigh numbers.

Nevertheless, these equations were proposed for stationary state. To measure heat transfer inside an enclosure in stationary state, experimental equipment must include a heat source and heat sink, to avoid temperature changes in the fluid. In the case of cylindrical shapes, correlations include two concentric cylinders as heat source and sink respectively. There is a general lack of transient or pseudostationary correlations for Nusselt number in vertical cylinders as enclosures. One exception could be the work proposed by Cherkasow (1985), who studied pseudostationary free convection in a cylinder heated from its sides or bottom. He correlated heat transfer as $Nu = aGr^{b}$, which, using a fixed Prandtl number, would be equivalent to a $Nu = aRa^{b}$ correlation. However this experiment was performed in a cylinder partially filled with a liquid instead of a gas (Gr=1.6×10^{7}). Therefore, this correlation cannot be applied to estimate heat transfer in our system.

2.3.4 Heat transfer in packed beds

Heat transfer in packed beds can be divided in many modes of conduction, and convection (and radiation, which won't be studied in the present work). Reviews on heat transfer in packed beds describe the following mechanisms (Adeyanju & Manohar 2009; Dixon 1985): (1) Convection between the wall and the fluid; (2) convection between the particles and the fluid; (3) conduction between the wall and the particle; (4) conduction between particles; and, (5) mixing of the fluid (*i.e.*, bulk convection). The relative significance of the heat transfer modes depends on the system studied. If the outer wall is adiabatic, the important modes will be axial conduction and convection from the particle to the fluid; but if this wall has a temperature gradient (as in the studied case), then wall to particle conduction and wall to fluid convection will be relevant as well.

Also, the relative relevance of heat transfer modes will depend on Biot number (*Bi*) that relates conduction inside the particle with convection between the particle and the fluid, as shown in Eq. (12):

$$Bi = \frac{h d_p}{k_s}, \tag{12}$$

where k_s is the solid conductivity. For example, if Biot number is small (Bi<0.1), then conduction inside the particles is very fast, and heat transfer from the particles to the fluid depends solely on convection between the particles and the fluid. Since most of the work reviewed by Adeyanju and Manohar (2009) proposed global coefficients for effective conductivity or global convective heat transfer, they recommend to check which model is better adapted to a specific application.

Heat transfer in a packed bed by effective conduction entails heat being transferred by conduction in parallel between the solid and the fluid phase (Dixon 1985). This model assumes that heat transferred due to the mixing of the fluid is lower than the heat transferred through the solid phase or comparable to it. The interphase resistances (*i.e.*, resistance in the wall, between particles) were included in the effective conductivity of the solid material. The effective conductivity without flow λ_e^0 can be calculated as a relationship between the conductivity of the solid λ_s and the conductivity of the fluid λ_f, as proposed by Krupiczka and reviewed by Wen and Ding (2006) (Eq. 13):

$$\lambda_e^0 = \frac{\lambda_s^m}{\lambda_f^{m-1}}, \text{ being} \tag{13}$$

$$m = 0.28 - 0.757\log(\varepsilon_e) - 0.057\log\left(\frac{\lambda_s}{\lambda_f}\right).$$

Then, in the presence of a crossflow, the effective conduction should be enhanced by some mixing of the fluid. Several authors (Wen & Ding 2006; Dixon 1985) propose enhancement factors for the effective (radial) conductivity λ_e, as function of the product of Reynolds and Prandtl numbers, as shown in Eq. (14):

$$\lambda_e = \lambda_e^0 + aRePr, \tag{14}$$

where the coefficient *a* was reported by different authors ranged between 0.1 and 0.5.

In cases when the mixing of the fluid is high, the conductivity of the solid material becomes less relevant, and the closest approach to calculate heat transfer is through correlations of the Nusselt number. Phanikumar and Mahajan (2002) state that a porous material can either enhance or impede convective heat transfer. If the conductivity of the solid is high, then heat transfer is enhanced due effective conduction in the solid phase parallel to the convection. On the other hand, when the conductivity of the solid material is small, the conduction is completely irrelevant for heat transfer, and only convection is presented. Depending on properties like porosity and tortuosity of the packed bed, convection will be more or less impeded in comparison to convection without any packed bed due to a reduction of the buoyant flow.

Correlations proposed for convection in packed media were reviewed by Bejan (1987). Studies have been done either under forced flow or under natural convection. Correlations for natural convection were proposed by many authors, being the majority of them of the form $Nu = aRa^{b}$. Unlike natural convection in a pure fluid, parameters for the correlation for convection in packed beds range more widely, $0.44 < a < 1.47$ and $0.25 < b < 0.5$. This high variability could be product of differences in the calculation procedure or differences in properties of the packed beds used in the experiments, like particle size and shape, porosity, among others.

3 MATERIAL AND METHODS

3.1 Preparation and characterization of samples

Four different substrates similar to those remaining in a vessel after supercritical extraction were produced. Rosehip and raspberry seeds deoiled by pressing were kindly provided by Granasur S.A. (Santiago, Chile). They were grinded and sieved (+4/-6 mesh) to obtain a uniform particle size. Substrates were pelletized in a PP85 pellet mill (PelletPros®, Dubuque, IO) with 4.5 mm openings. Pellets were cut into cylinders *ca.* 4.5 mm long. The four substrates were deoiled using 19 kg of CO_2 at 60 ºC and 30 MPa (*i.e.*, the conditions chosen for decompressions) per 1 kg sample. Table 3-1 tabulates the moisture of the samples after extraction using a Sartorius (Göttingen, Germany) MA 30 infrared balance, and the residual content of oil of the samples (measured by Soxhlet extraction with *n*-hexane).

Table 3-1. Moisture and residual oil content of supercritical CO_2 extracted substrates.

Substrate	Moisture (% w.b.)	Residual oil content (% d.b.)
Pressed rosehip	4.9	0.4
Pelletized rosehip	3.5	0.5
Pressed raspberry	5.8	0.7
Pelletized raspberry	4.5	0.4

Particle size distributions were measured using image analysis as described by Mauguet *et al.* (Mauguet et al. 2005). A sample of about 100 to 200 particles was photographed with a Powershot® SD900 camera (Canon, Tokyo, Japan). Images were analyzed with the software ImageJ (The National Institutes of Health, Bethesda ML). The equivalent diameter d_p was calculated as the diameter of a circle with the same projected area A_p, Eq. (15):

$$d_p = \sqrt{\frac{4A_p}{\pi}} \tag{15}$$

Intraparticle porosity ($\varepsilon_i = 1 - V_{solid}/V_{particle}$) and interparticle porosity ($\varepsilon_e = 1 - V_{particle}/V_{bulk}$) were determined using relationships between densities, as described by Mauguet *et al.* (Mauguet et al. 2005). An Ultrapyc 1200e gas pycnometer (Quantachrome®, Boynton Beach, FL) was used to measure solid (true) density ρ_s. Alumina powder (50-µm particle size) was used to measure particle density ρ_p by displacement, as described by Mauguet *et al.* (2005). Bulk density ρ_b was estimated as the ratio between the weight of substrate loaded and the empty volume of the high-pressure vessel described in Subsection 3.2 during packing. Intraparticle porosity, Eq. (2), interparticle porosity, Eq. (3), and total porosity, Eq. (4), were calculated as described in Subsection 2.2.

The effective thermal conductivity of the substrates λ_b was measured using a Lambda 50 device (Eurotechnica GmbH, Bargteheide, Germany). This device compares the conductivity of a sample with the conductivity of a reference material. The sample and a 14-mm thick disc of PMMA having a thermal conductivity of 0.195 W m^{-1} K^{-1} are stacked between the heating and cooling elements that produce a temperature gradient, interposing copper discs with thermocouples. Since heat flux is equal for both resistances in series, the heat transfer equations are combined in Eq. (16):

$$\lambda_b = \lambda_r \left(\frac{\Delta T_r}{x_r} \right) \frac{1}{\left(\Delta T_b / x_b \right)}, \tag{16}$$

where ΔT_b and x_b are the temperature gradient around the sample and the sample's thickness; and λ_r, ΔT_r, and x_r are the reference's thermal conductivity, the temperature gradient around the reference, and the reference's thickness.

3.2 Equipment, instrumentalization and experimental procedure

Figure 3-1 shows the equipment built to measure temperatures, pressures, and flow rates during decompressions. An Autoclave Engineers AH-1496 (Erie, PA) one-gallon

reactor (1) was connected by a three-gate valve (2) to either the pumping system or the venting line. A 5.6-m heating coil (3), a 15F-11NFB needle valve (4) with a micrometering handle (HiP, Erie, PA), and a 0.5-µm pore diameter filter (5) were placed between the three gate valve and the vessel. A heating bath (6) circulated water through the jacket of the high-pressure vessel, the heating coil, and the micrometering valve's seat. The water's inlet and outlet temperatures were measured with type K thermocouples (TR1 and TR2, respectively), and its flow was measured with a standard water rotameter (FM1). Temperatures of the CO_2 were measured at the exit of the vessel (TR3) and before the three-gate valve (TR4) with type K thermocouples. Pressures of the CO_2 at these same points (PR1 and PR2, respectively) were measured with DMP 331 pressure transmitters (BD sensors, Thierstein, Germany). All temperature and pressure sensors were connected to a Multicon v.2.23.0 (Eurotechnica GmbH, Bargteheide, Germany) data logger (not shown in the figure). A p200 (Thar Technologies, Pittsburgh, PA) pump (7) pressurized CO_2 stored in a cylinder (8) and cooled in a 12 m coil (9). Antifreeze solution from a 15 L chiller (10) (Polyscience, Niles, IL) cooled both the coil and the pump's piston heads. The venting line allowed switching between a H271B-010 (Headland, Atlanta, GA) flow meter (FM2) and a standard gas rotameter (FM3) to measure between 4 and 70 standard liter per minute.

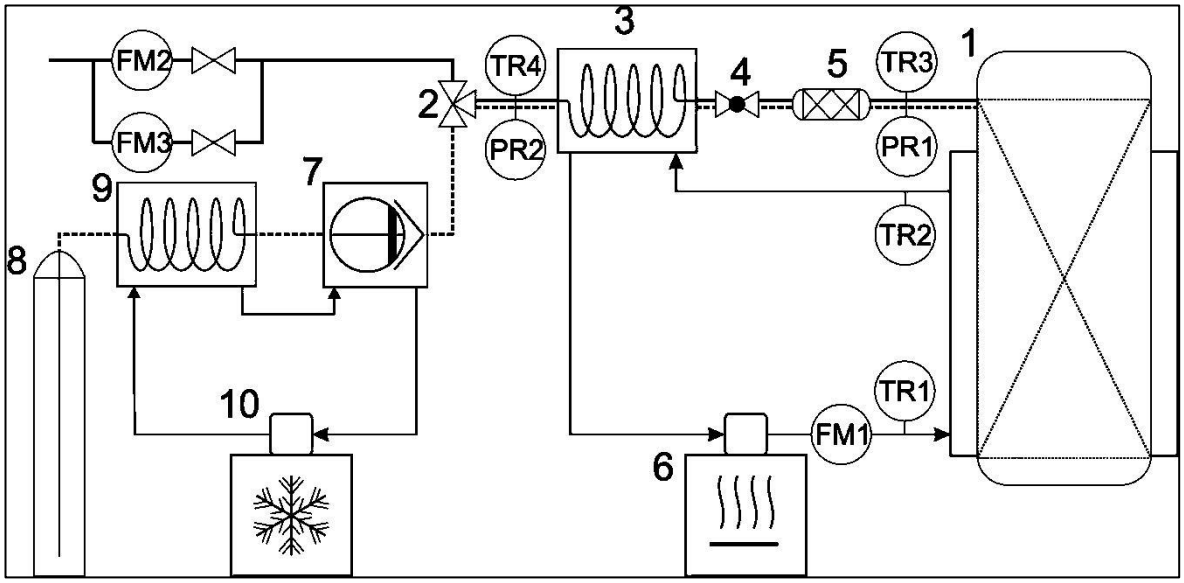

Figure 3-1. Components, piping, and measuring instruments of the system arranged to measure decompressions: (1) High-pressure vessel; (2) Three-gate valve; (3) Heating coil; (4) Micrometering valve; (5) Filter; (6) Heating bath; (7) Piston pump; (8) CO_2 cylinder; (9) Cooling coil; (12) Cooling bath; (TR1-TR4) Type K thermocouples; (PR1 and PR2) Pressure transmitters (0-60 MPa); (FM1) Water rotameter; (FM2) Gas flow meter (7-70 standard liter per minute); and, (FM3) Gas flow meter (4-40 standard liter per minute).

Figure 3-2 shows the high-pressure vessel adapted for the decompression experiments. The inner volume of the vessel was 3.96 L and its weight (*i.e.,* walls, bottom, lid, screws, and direct fittings) was 66.0 kg. A 22-mm wide jacket with a 30-mm pitch helicoid covered the side of the vessel. Three type K thermocouples placed inside a 6.3-mm OD tube along the central axis of the vessel (*i.e.* T1, T2, and T3), and two more freely placed at 30 mm of the wall (*i.e.* T4) and at the vessel's wall (*i.e.* T5), were connected to the data logger (*cfr* Appendix 1 for the calibration of the thermocouples). The vessel was insulated with 19-mm thick Aeroflex® MSR (Samutprakan, Thailand).

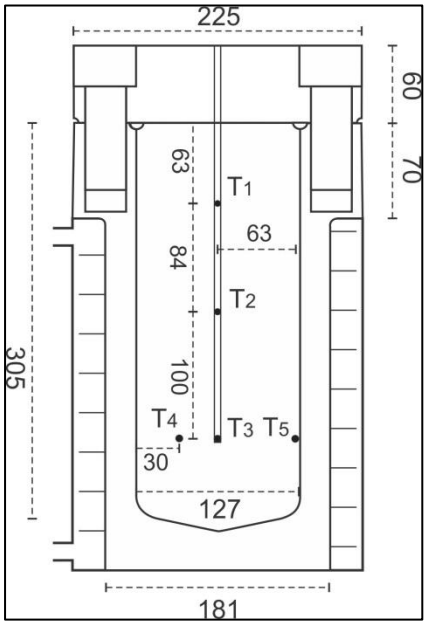

Figure 3-2. Geometry of the high-pressure vessel: (T1-T3): Type K thermocouples intubed at the axial center of the vessel; and, (T4 and T5) Type K thermocouples freely placed in the vessel (measures in mm).

Decompression experiments consisted in charging the vessel with supercritical CO_2, waiting to equalize its inner temperature and pressure, and venting the CO_2. To charge the vessel, CO_2 was cooled at -5 ºC and then pumped at 100 g/min up to the desired initial pressure. The heating bath was set to the desired initial temperature while the micrometering valve was fully open. To compensate pressure changes due to temperature equalization, CO_2 was either pumped in or vented out during this process. In about 30 minutes the required steady state conditions were reached (*i.e.*, neither a change in inner temperature nor a difference between inlet and outlet temperature of the water in the vessel's jacket were observed). For venting, the micrometering valve was fully closed and the three-gate valve was changed to connect the vessel to the venting line. Then the micrometering valve was opened to either 0.3 turns (hence slow venting) or 0.6 turns (hence fast venting) and kept constant while venting. The heating bath was set at the initial temperature during decompressions as well.

3.3 Experimental design

The effects of the valve opening, initial temperature, and substrate packed in the high-pressure vessel were studied in decompressions starting at 30 MPa. Four conditions were chosen for decompressions with empty vessel (without any substrate charged), consisting of an initial temperature of either 50 or 60 ºC combined with either a slow or fast venting. These conditions were chosen to avoid the formation of two-phase fluid in the vessel. An initial temperature of 60 ºC and slow venting were chosen for replicas. For decompressions of a packed bed (a vessel charged with substrate), the substrates described in Subsection 3.1 were randomly charged. An initial temperature of 60 ºC and slow venting were chosen for decompressions of packed beds, and replicas were done with pressed rosehip.

Temperatures and pressures were recorded every 10 seconds. Vented flow and heating water flow were registered manually every minute, and values for 10-s intervals were interpolated as required (*cfr.* Appendix 2 for calibration of vented flow measurement). All thermophysical properties of CO_2 (*i.e.*, density, internal energy, enthalpy) were estimated as a function of temperature and pressure using NIST Database (Lemmon et al. 2007).

3.4 Statistical analysis and calculations

A multifactorial analysis of venting time and temperature drop in decompressions of an empty vessel was carried out using Statgraphics Centurion XVI software, version 16.1.11 (Statpoint Technologies, Warrenton, VA). The significance of the difference between curves was determined by comparing them with the standard deviations of experiments.

Mass flow rate of the vented CO_2 F was obtained from volumetric flow rate and the density as a function of pressure and temperature after expansion. Remaining mass in the vessel was integrated backwards from the mass flow rate, Eq. (17):

$$M_{t-1} = M_t + F\ \Delta t\,, \tag{17}$$

where M_{t-1} and M_t are the CO_2 mass in the vessel before and after flow measurement, and Δt the time interval (*i.e.*, 10 s). The initial mass in the vessel M_o was calculated with the density of CO_2 at the initial conditions. A correction factor was applied to the vented mass flow rate to fit the total integrated mass flow with the initial mass charged in the vessel (*cfr* Appendix 2).

The internal energy of the CO_2 in the vessel was calculated using the integral form of the heat balance for transient systems described by Himmelblau and Riggs (2011). Since net accumulation of heat in the walls, bottom, and lid of the high-pressure vessel could not be calculated, only the change in internal energy of the CO_2, the heat transferred from the substrate and heating bath to the CO_2, and the enthalpy lost with the vented current were quantified in Eq. (18):

$$M_t u_t = M_{t-1} u_{t-1} + \left(F_h c_{ph} \Delta T_h - F\ h_v \right) \Delta t - m_s c_{ps} \left(\bar{T}_t - \bar{T}_{t-1} \right), \tag{18}$$

where u_{t-1} and u_t and are the specific internal energies of the CO_2 in the vessel before and after measurement, F_h is the flow rate of the heating water, c_{ph} is the specific heat of water, ΔT_h is the temperature difference of the heating water between inlet and outlet current, and h_v is the specific enthalpy of the vented CO_2 before its decompression. The term $m_s c_{ps} \left(\bar{T}_t - \bar{T}_{t-1} \right)$ refers to the sensible heat transferred from the substrate of weigh m_s at the mean temperatures inside the vessel of $\bar{T}_t$ and $\bar{T}_{t-1}$, respectively. The specific heat of the substrates c_{ps} was estimated using the Choi-Okos correlation for food materials reviewed by Sweat (1994) using their proximal compositions found in literature (Ilyasoğlu 2014; Bushman et al. 2004). The initial internal energy of the CO_2 was calculated with the mean properties in the vessel. Rearranging Eq. (18) for the heat added to the system through the vessel's inner walls Q, an internal heat transfer coefficient U can be calculated from the temperatures at the inner wall of the vessel T_w and the bulk of the vessel $\bar{T}$ and the transfer area A (*i.e.*, the area of the cylindrical wall of the vessel), Eq. (19):

$$Q\big|_{\mathrm{t}} = \Big[U\ A\ \left(T_{\mathrm{w}} - \bar{T}\right)\Big|_{\mathrm{t}} = \frac{\left(M_{\mathrm{t}} u_{\mathrm{t}} - M_{\mathrm{t-1}} u_{\mathrm{t-1}}\right) + m_{\mathrm{s}} c_{\mathrm{ps}} \left(\bar{T}_{\mathrm{t}} - \bar{T}_{\mathrm{t-1}}\right)}{\Delta t} + \Big[F\ h_{\mathrm{v}}\big|_{\mathrm{t}} \,. \tag{19}$$

4 RESULTS

Results are divided in three subsections. Subsection 4.1 describes temperature and pressure evolution for decompressions of empty vessels. Subsection 4.2 describes temperature and pressure evolution for decompressions of packed vessels. Finally, Subsection 4.3 compares the mass balance, energy balance, and heat transfer with the theoretical background to ascertain the mechanisms defining momentum and heat transfer to a high-pressure vessel during decompression.

4.1 Pressures and temperatures for decompressions of empty vessel

Figure 4-1 shows temperatures and pressure *versus* time for decompression of an empty vessel with a slow venting starting at 60 ºC (*cfr.* Appendix 3 for decompressions of a vessel at other starting temperatures and valve openings). Three stages were observed, the same as in the experiments of Gebeken and Eggers (1995) using supercritical CO_2, although there was no phase change in our experiments. Pressure and temperatures descended sharply in the first stage. In the second stage, pressure descended slowly and temperatures remained comparatively constant. The bulk temperatures differentiated from the wall temperature in the third stage. All bulk temperatures were statistically similar during the whole decompression. Therefore, the mean value of all bulk temperatures was used in empty vessels to describe the temperature of the CO_2. Unlike in our experiments, when decompressing a gas-liquid mixture of saturated CO_2, Eggers and Green (Eggers & Green 1990) observed that bulk temperatures were homogeneous and equal to the wall temperature only below the gas-liquid interphase, where conditions of liquid CO_2 were measured. They observed axial differences in bulk temperature, because the gas-liquid interphase descended in time.

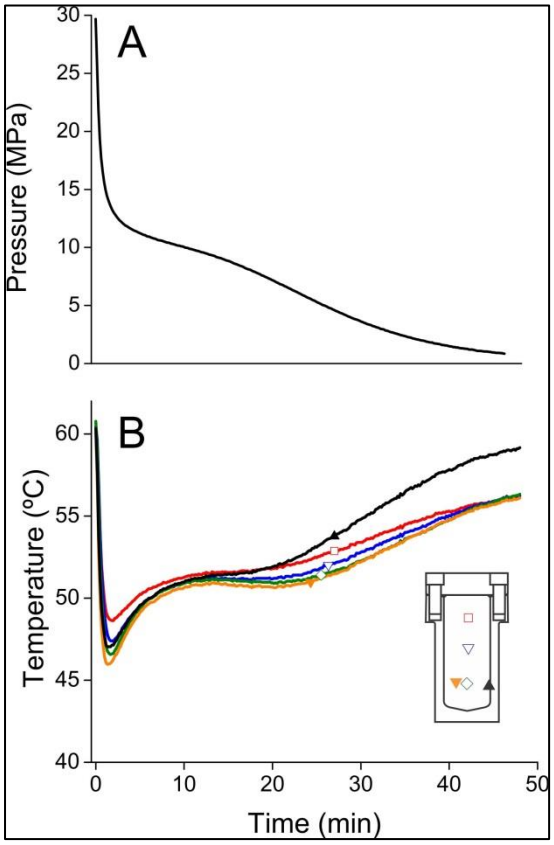

Figure 4-1. Changes in (A) pressure (± 0.5 MPa) and (B) temperatures (± 0.7 ºC) as a function of decompression time for slow (C_v = 0.003, corresponding to 0.3 turns of the valve handle) decompressions starting at high temperature (60 ºC) in a high-pressure vessel with pure CO_2.

Figure 4-2 compares decompressions as a function of initial temperature and decompression rate. The multifactorial analysis revealed that valve opening and initial temperature had a significant effect ($p \leq 0.05$) in decompression time, whereas only the initial temperature had a significant effect ($p \leq 0.05$) in it. Increasing venting rate reduced the time to reach 1.5 MPa in 56%, and increased the drop in temperature in 41% (using a ºC scale). Increasing the initial temperature reduced decompression time in 29%, without a change in the drop in temperature. In fact, temperature versus time curves with the same valve opening but different initial temperatures have the same shape, but in a different vertical position). The effect of initial temperature on

decompression time was observed also by Gebbeken and Eggers (1995) and can be explained by the lower density of CO_2 at higher temperatures.

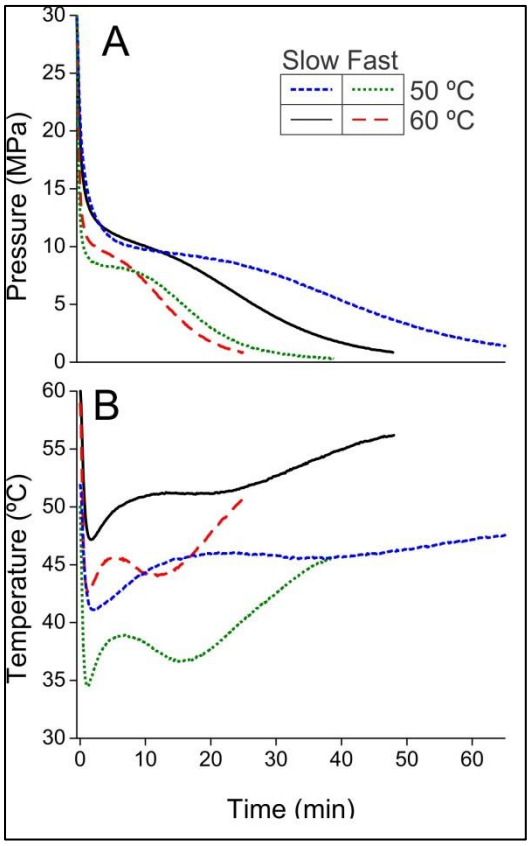

Figure 4-2. Changes in (A) Pressure and (B) Mean temperature as a function of decompression time for different decompression rates (C_v = 0.003 for Slow venting; or C_v = 0.006, corresponding to 0.6 turns of the valve handle, for Fast venting) and initial temperatures (50 or 60 ºC) in a high-pressure vessel with pure CO_2.

Figure 4-3 shows the temperatures of all decompressions *versus* pressure. Transitions between the three stages of decompressions were related with thermophysical properties of CO_2. Temperature in the first stage dropped near to the adiabatic line (*i.e.*, points with the same internal energy as the initial conditions of decompression) regardless of the valve opening or the initial temperature. Decompressions were initially so fast that heat transfer from the vessel walls was insufficient to maintain a constant temperature. At the second stage temperatures rose from the adiabatic temperature, indicating that heat transfer counterweighted the drop in temperature. The third stage was marked by the

surpassing of the pseudocritical line. The differences between bulk and wall temperatures indicated that the properties of CO_2 at this stage provided actually a poor heat transfer from the vessel walls to the fluid.

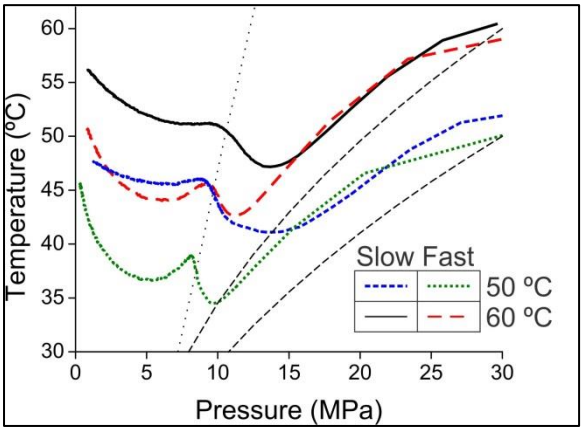

Figure 4-3. Mean temperature as a function of pressure for different decompression rates (C_v = 0.003 for Slow venting, or C_v = 0.006 for Fast venting) and initial temperatures (50 or 60 ºC) in a high-pressure vessel with pure CO_2 in comparison with the adiabatic lines (– – –) and the pseudocritical line (·····).

4.2 Pressure and temperatures for decompressions with packed beds

Table 4-1 list the physical properties of the substrates. Although pelletized substrates had larger equivalent diameters than pressed substrates, all samples had equivalent diameters d_p small enough in comparison to the diameter of the high-pressure vessel D ($18.4 \leq D/d_p \leq 22.7$) to be considered as homogeneous beds (Roblee et al. 1958; Thadani & Peebles 1966). The solid densities of all substrates were alike. Pelletization increased particle density and bulk density, and decreased interparticle porosity and total porosity. Intraparticle porosity was higher for rosehip than raspberry, and did not vary with samples pretreatment; this can be related with the oil content of the substrates before extraction (72 and 44 g/kg for rosehip and raspberry, respectively). Compared to literature correlations for interparticle porosities of regular particles (Roblee et al. 1958; Thadani & Peebles 1966), pellets had a porosity similar to packed bed of cylinders (0.37), whereas pressed substrates had a higher porosity than packed beds of spheres

(0.40). Effective thermal conductivity increased slightly due to pelletization, but in all cases neared the thermal conductivity of CO_2.

Table 4-1. Physical properties of the substrates used in this work.

Physical property	Pressed rosehip	Pelletized rosehip	Pressed raspberry	Pelletized raspberry
Equivalent diameter (mm)	$6.1^{b.*}$	6.9^{d}	5.6^{a}	6.7^{c}
Solid density (kg/m^3)	$1410^{a.b}$	1430^{b}	1380^{a}	1420^{a}
Particle density (kg/m^3)	1000^{a}	1100^{b}	1160^{c}	1160^{c}
Bulk density (kg/m^3)	498	688	549	711
Intraparticle porosity (–)	0.30^{b}	0.23^{b}	0.16^{a}	0.18^{a}
Interparticle porosity (–)	0.50	0.37	0.53	0.39
Total porosity (–)	0.65	0.52	0.60	0.50
Effective thermal conductivity (W m^{-1} K^{-1})	0.10^{a}	0.13^{b}	0.14^{c}	0.18^{d}

* The same letter in a single row indicates that values of the property are not significantly different ($p > 0.05$).

Figure 4–4 shows decompression of a high-pressure vessel charged with pressed rosehip (*cfr.* Appendix 4 for decompressions of a vessel filled with other substrates). Decompression in this case followed the same three stages described for empty vessels in Subsection 4.1. The packed bed reduced decompression time and the drop in temperature in the first stage as well. Eggers and Green (1990) observed also this effect, and explained that a packed bed reduces the amount of CO_2 initially filled in the vessel and stores energy as sensible heat. During the third stage, bulk temperatures descended again, and local differences appeared. Temperatures on the upper portions of the vessel were higher than temperatures at the bottom. Temperature T4 at a position closer to the vessel wall than T3 was the lowest, which could not be explained by the authors.

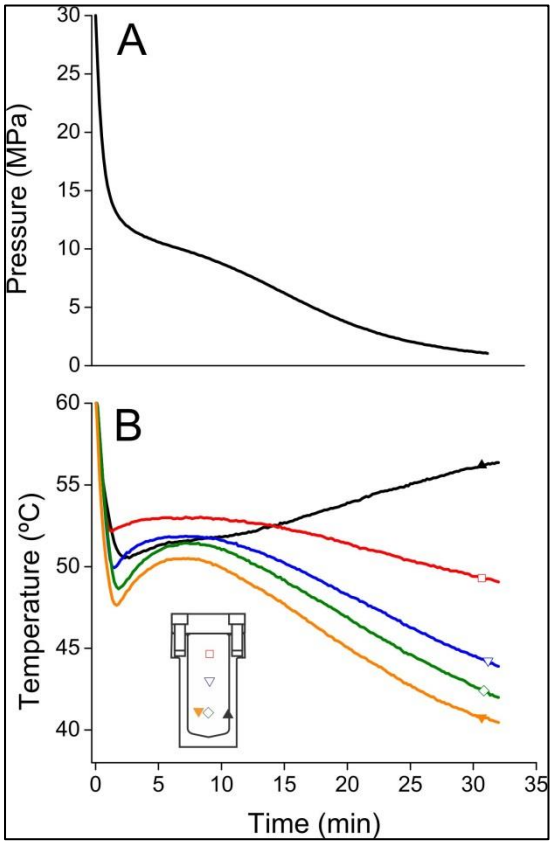

Figure 4-4. Changes in (A) Pressure (± 0.2 MPa) and (B) Temperatures (± 1.0 ºC) of CO_2 as a function of decompression time for slow (C_v = 0.003) decompressions starting at high temperature (60 ºC) in a high-pressure vessel packed with pressed rosehip.

Independent on the substrate charged, the CO_2 in the high-pressure vessel had similar decompression curves. Decompressions with packed beds differed in their duration. The vessel packed with pelletized raspberry took 24 min to reach 1.1 MPa, whereas the one packed with pressed rosehip took 32 min. This difference was proportional to the amount of CO_2 initially charged (*i.e.*, the total porosity). Plotted against dimensionless time (*i.e.*, time divided by total decompression time), Figure 4-5 (A) shows that no factor other than the porosity appeared to affect the drop in pressure in decompressions using different substrates. In a similar way, Figure 4-5 (B) shows the evolution of the temperature inside the vessel *versus* dimensionless time. As the temperature inside the vessel, the average of T2 and T3 (the two lowest axial temperatures) was considered because they were statistically similar during the whole experiment (Figure 4-4).

Temperatures *versus* dimensionless time were statistically similar for all packed beds, regardless of the thermal conductivity of the substrates.

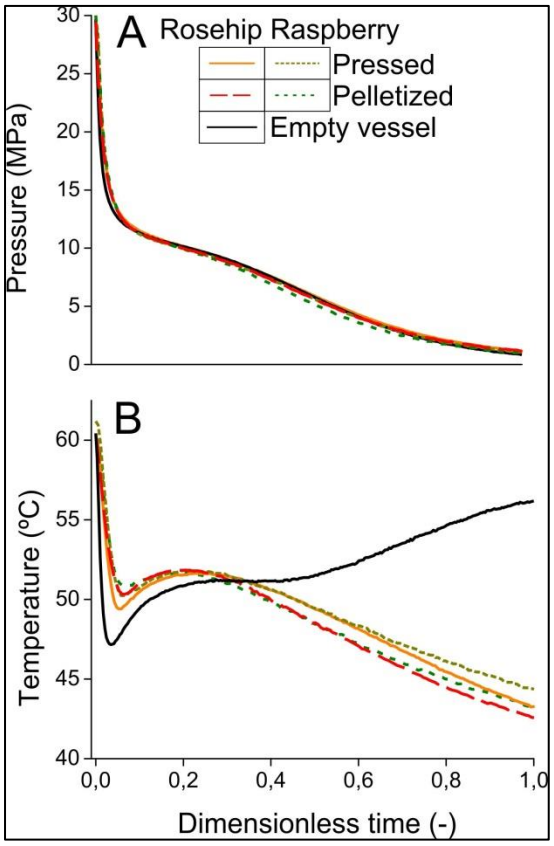

Figure 4-5. Changes in (A) Pressure and (B) Mean temperature of CO_2 as a function of decompression time for slow (C_v = 0.003) decompressions starting at high temperature (60 ºC) in a high-pressure vessel packed with different substrates.

Figure 4-6 shows the temperature *versus* pressure of decompressions of packed vessels. Although a similar drop in temperature was observed in the first stage of decompression, temperatures in packed vessels did separate from the adiabatic line more than temperatures in empty vessels (compare Figure 4-6 with Figure 4-3). This was probably due to the large amount of heat transferred from the substrate due to its large specific surface. The sharp drop in temperature at the third stage coincided with the surpassing of the pseudocritical line. No significant difference was observed between substrates, despite differences in thermal conductivities between them.

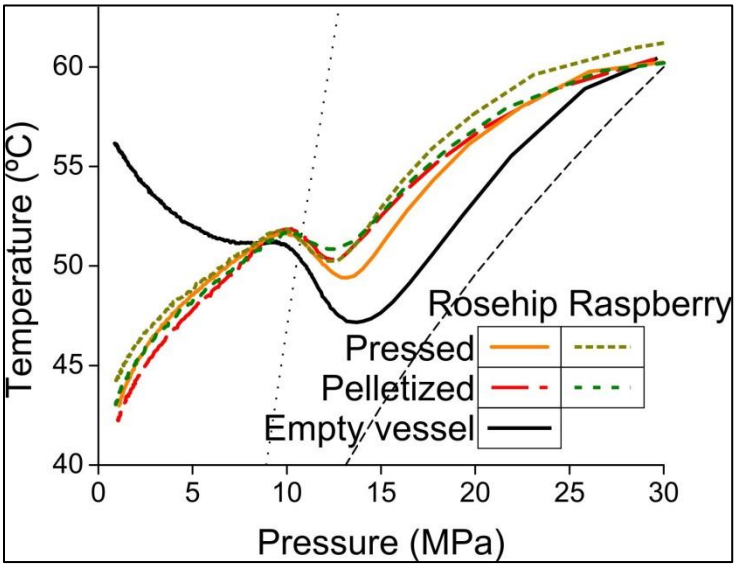

Figure 4-6. Mean temperature of CO_2 as a function of pressure for slow (C_v = 0.003) decompressions starting at high temperature (60 ºC) in a high-pressure vessel packed with different substrates in comparison with the adiabatic lines (– – –) and the pseudocritical line (·····).

4.3 Mass balance, energy balance and heat transfer

Vented flow appeared to behave like a choked flow in the valve's seat. Previous modeling of decompressions of supercritical fluids calculated a critical mass flux and fitted the venting area to a constant value (Zhang et al. 2014). Particularly, flow in a venting needle valve behaves as chocked flow if the pressure drop is high (Long & Guan 2011). A compressible flow through a nozzle becomes chocked when the velocity of the fluid at its exit equals the speed of sound and the flow does not increase as a result of a decrease in downstream pressure (Oosthuizen & Carscallen 2014). Figure 4-7 plots mass flow rate against choked mass flux (*i.e.*, the product between sound speed and density at the vessel's exit). A linear relationship between flow rate and chocked flux was observed, where fast venting curves differed from slow venting curves, and the slope of the regression can be related to the area of an orifice that restricts the flow rate similarly to the valve. These equivalent areas were 18.4×10^{-3} mm^2 for slow venting and 39.1×10^{-3} mm^2 for fast venting, respectively. The predicted areas were much smaller than the areas

of orifice plates used by Gebbeken and Eggers (1996), but their experiments had larger flow rates as well.

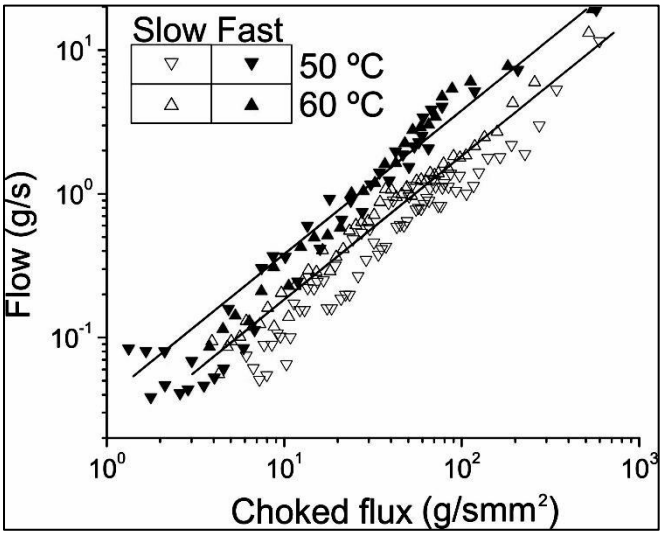

Figure 4-7 Linear regression between vented mass flow rate and choked mass flux (*i.e.* the product between the density and the speed of sound) of the CO_2 at the seat of the valve.

Added heat did not fit the change in internal energy of CO_2 in the system, unless heat accumulation in the walls of the high-pressure vessel was considered. This internal energy as well as the integrated heat descended with time due to the enthalpy loss with the vented current, as shown in Figure 4-8A. Although heat yielded by both the heating jacket and the packed bed raised the internal energy significantly, it was not enough to close the energy balance of CO_2. This can be explained by the net accumulation of heat in the steel of the wall, bottom, and lid of the high-pressure vessel. In fact, Green (1991) measured temperatures within the wall of the vessel at different depths, concluding that mean temperature in the wall dropped 35 ºC for a 38 min decompression. A mean temperature was estimated for the walls of the high-pressure vessel (*i.e.*, assuming that its bottom and lid were adiabatic) and the whole vessel as shown in Figure 4-8B. These mean temperatures were higher for decompressions of packed than empty vessels (*cfr* Appendix 5), due to the lower amount of CO_2 vented and the heat yielded by the substrate. In the experiment with an empty vessel, the mean temperature calculated only

for the walls of the high-pressure vessel sank lower than the minimum temperature of the inner wall, and therefore the assumption of adiabatic lid and bottom was discarded. Although the mean temperature calculated for the whole extractor was lower than the temperature in the inner wall of the vessel at the end of the experiments, it must be accounted that the vessel's lid and bottom did not have any jacket, and therefore were not heated from the jacket again.

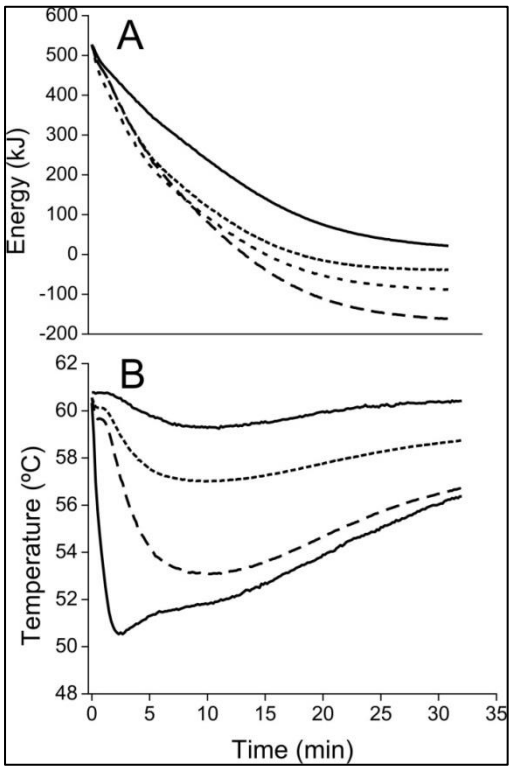

Figure 4-8 (A) Energy balance for CO_2 as a function of decompression time for slow (C_v = 0.003) decompressions starting at high temperature (60 ºC) in a high-pressure vessel packed with pressed rosehip. Legend: (—) Internal energy of the CO_2; (----) Heat yield by the packed bed + heat yield by the heating bath – enthalpy lost with the vented current; (- -) Heat yield by the packed bed – enthalpy lost with the vented current; and, (— -) Heat yield by the heating bath – enthalpy lost with the vented current. (B) Estimated mean temperature of the steel of the walls of the high-pressure vessel as a function of decompression time for decompressions starting at 60 ºC in the high-pressure vessel packed with pressed rosehip. Legend: (- -) Estimated temperature of the steel asuming that the whole vessel yields heat to the CO_2; (— -) Estimated temperature of the steel asuming that only the walls of the vessel yields heat to the CO_2; and, (—) Inner and outer walls of the high-pressure vessel.

Figure 4-9 compares experimental values of the heat transfer coefficient for decompression of empty and packed vessels to literature correlations for natural convection in liquids and gases, and effective conduction. In the case of empty vessels, experimental data was compared to Ede's correlation for natural convection in vertical plates under laminar flow conditions that was reviewed by Kaviany (1994), given that the diameter of the high-pressure vessel was 10 times thicker than the boundary layer for buoyancy (Kaviany 1994). As expected for the enhancement of heat transfer under supercritical conditions proposed by several authors (Green & Eggers 1991; Bae 2011; S. M. Liao & Zhao 2002), the correlation for liquids and gases underestimated heat transfer in the super- and near-critical state in our experiments. Heat transfer in packed vessels fitted the effective conduction correlation of Dixon (1985) only in the third stage of decompression. The measured heat transfer coefficient at supercritical conditions appeared like the attenuated convective heat transfer described by Phanikumar and Mahajan (Phanikumar & Mahajan 2002) for porous media.

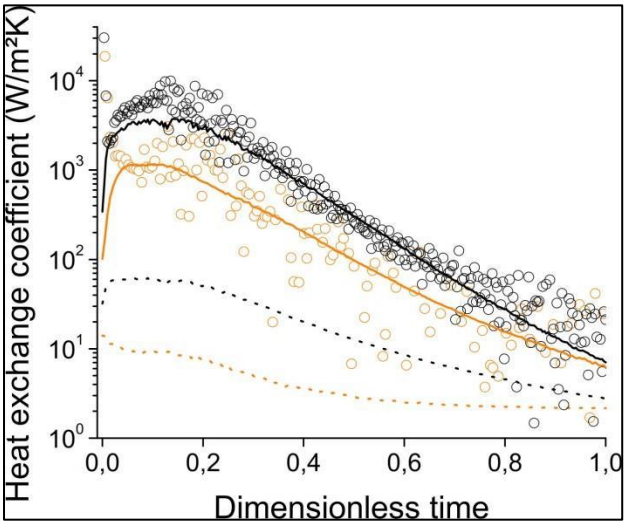

Figure 4-9. Heat transfer coefficient for decompression of empty vessel (○) and packed vessel (○) compared to correlation for natural convection in normal fluids (· · ·), correlation for effective conductivity in packed beds (· · ·), and correlation proposed by authors for natural convection in supercritical fluids with best-fitted parameters (— —).

Given the lack of a suitable correlation for natural convection in supercritical fluid, a regression of $Nu = a\ Ra^{b}$ was proposed, where *Nu* and *Ra* are the dimensionless Nusselt and Rayleigh numbers, and *a* and *b* are best-fitting parameters. The obtained correlations were $Nu = 1.73\times10^{-4}\ Ra^{0.71} \pm 9.10\times10^{-3}$ for empty vessels, and $Nu = 1.90\times10^{-4}\ Ra^{0.63} \pm 5.30\times10^{-3}$ for packed vessels (*cfr* Appendix 6 for the regression of the Nusselt number in empty and packed vessels as a function of the Rayleigh number). The stronger dependence on the Rayleigh number than literature correlations reflects the aforementioned enhancement of heat transfer in supercritical fluids.

5 DISCUSSION

Regarding the conditions of the decompression, venting rate affects directly the decompression time and drop in temperature; a higher initial temperature only shortens the decompression time, due to the smaller amount of CO_2 stored initially in the vessel. The venting conditions applied are probably impractical for industrial processes, because of our need to avoid formation of two phases in the high-pressure vessel to allow computations of density and internal energy during decompression. If the venting area of the decompressions of Gebbeken and Eggers (1996) were matched, decompressions would have been about 30 times faster. Temperatures would have dropped to very low levels and the adiabatic stage of decompression would have crossed the saturation line. Obviously, this is another extreme that is not practical for industrial decompressions either; the optimal venting condition for each initial temperature would be between these two cases.

Regarding the packed substrate, it can be concluded that only the total porosity had an effect on the pressure descent, and changes in temperature change the decompression. Principally, the theory that the effective conductivity of the substrate could rise the internal temperature in the vessel was discarded, indicating that the substrate worked as an insulator and a heat reservoir. While internal temperatures at decompressions of empty vessels were homogeneous, axial and radial differences in temperature were observed for decompressions of packed vessels. Decompressions of packed vessels should do less damage to the material of the vessel, because the changes in the estimated mean temperature of the steel of the high-pressure vessel was lower in this case, than in decompressions of empty vessel (where it was about 5 ºC smaller, data not shown).

The decompression of larger extraction vessels could be simulated mathematically, considering the principles observed in our experiments. Choked flow in the valve should be used to model the venting flow, varying the venting area if necessary. The mass conservation should consider the vented flow; while the energy conservation should consider the heat yielded from the jacket, the packed bed, and the steel of the high-

pressure vessel besides the enthalpy loss with the vented current. It is important to remark that unless the lid and bottom of the vessel were a small fraction of the mass of the vessel, they should be taken into account to calculate the internal energy in the vessel.

Heat appeared to be transferred by convection even in packed vessels. Since there is no literature correlation for the heat transfer coefficient suiting the conditions of the studied system nor the experimental values, correlations based on the dimensionless Rayleigh number were proposed, whose precision was however limited. If a mathematical simulation were to be developed, more precise values of the heat transfer coefficient should be correlated.

6 CONCLUSIONS AND PERSPECTIVES

The present work fulfilled the proposed objectives. It was observed that the proposed mass and energy balance could explain the evolution of a decompression of high-pressure vessels. The principle of chocked flow was an important discover for modelling the decompression process, as well as the observation that heat transfer was much higher in supercritical fluids compared with gases or liquids. In fact, the author had the chance to codirect the work in modeling decompressions of high-pressure vessels as well. This work advance was in concordance with experiments of decompressions; for example, the principle of chocked flow was applied to the mass balance, improving substantially pressure evolution during decompressions.

The future work in this topic should center in determining a suitable heat transfer correlation for supercritical fluids in an enclosure. The proposed correlation still had a too high variability. Moreover, since the packed materials had similar thermal properties, no influence of the packed bed could be observed. To better understand the heat transfer phenomena in decompressions of packed vessels, experiments with model materials are proposed.

Porous stainless steel was generated to emulate natural substrates. A screening of metallic foams with different porosities and pore sizes was generated; the combination that resembled vegetable substrates the most was replicated. These cylinders have a controlled and homogeneous size, shape, and pore distribution. These materials will be used both to study heat transfer in decompression of packed vessels, and to study mass transfer in ScFE. Preliminary test of impregnation and extraction of model materials with supercritical Sc CO_2 showed a “clean” extraction curve; it is expected that estimations of heat transfer coefficients will be precise as well.

NOMENCLATURE

Latin letters

A	Area (m^2)
c_p	Specific heat (kJ kg^{-1} K^{-1})
D	Diameter (m)
F	Mass flow rate (kg/s)
Gr	Dimensionless Grashof number ()
h	Specific enthalpy (kJ/kg)
k	Convective heat transfer coefficient (kJ m^{-2} K^{-1})
m	Mass (kg)
M	Mass of CO_2 in the vessel (kg)
Nu	Dimensionless Nusselt number ($Nu = \frac{hL}{k_f}$)
Pr	Dimensionless Prandtl number ($Pr = \frac{c_p \mu}{k}$)
Q	Heat (kJ/s)
R	Radius (m)
r	Radial position (m)
Ra	Dimensionless Rayleigh number ($Ra = GrPr$)
Re	Dimensionless Reynolds number ($Re = \frac{v\rho L}{\mu}$)
S	Surface (m^2)
T	Temperature (ºC)
t	Time (s)
u	Specific internal energy (kJ/kg)
V	Volume (m^3)
v	Velocity (m/s)
x	Thickness (m)
Y	Height (m)
y	Axial position (m)

Greek letters

Δ	Differential
ε	Porosity
λ	Conductivity (W m^{-1} K^{-1})
ρ	Density (kg/m^3)
μ	Dynamic viscosity, (Pa s)

Subscripts

b	Bulk
bl	Boundary layer
d	Dust
e	Interparticle
forced	Forced component of Nusselt number
h	Heating bath current
i	Intraparticle
natural	Natural component of Nusselt number
p	Particle
r	Reference
s	Solid
t	Time
v	Vented current (before decompression)
w	Wall

REFERENCES

Adeyanju, A.A. & Manohar, K., 2009. Theoretical and experimental investigation of heat transfer in packed beds. *Research Journal of Applied Sciences*, 4, p.166–177.

Bae, Y.Y., 2011. Mixed convection heat transfer to carbon dioxide flowing upward and downward in a vertical tube and an annular channel. *Nuclear Engineering and Design*, 241, p.3164–3177.

Bejan, A., 1987. Convective heat transfer in porous media. In S. Kakaç, R. K. Shah, & W. Aung, eds. *Handbook of Single-phase Convective Heat Transfer*. New York NY: John Wiley & Sons, p. 1–34.

Benyahia, F. & O'Neill, K.E., 2005. Enhanced voidage correlations for packed beds of various particle shapes and sizes. *Particulate Science and Technology*, 23, p.169–177.

Brunner, G., 2005. Supercritical fluids: technology and application to food processing. *Journal of Food Engineering*, 67, p.21–33.

Bushman, B.S. Phillips, B., Isbell, T., Ou, B., Crane, J.M. & Knapp, S.J., 2004. Chemical composition of caneberry (Rubus spp.) seeds and oils and their antioxidant potential. *Journal of Agricultural and Food Chemistry*, 52, p.7982–9787.

Cherkasow, S.G., 1985. Natural convection in a vertical cylindrical vessel with heat supplied to its side and free surface. *Fluid dynamics*, 19, p.902–906.

del Valle, J.M., 2015. Extraction of natural compounds using supercritical CO_2: going from the laboratory to the industrial application. *Journal of Supercritical Fluids*, 96, p.180–199.

del Valle, J.M. & Aguilera, J.M., 1988. An improved equation for predicting the solubility of vegetable oils in supercritical CO_2. *Industrial & Engineering Chemistry*, 27, p.1551–1553.

del Valle, J.M. & Aguilera, J.M., 1999. Revisión: extracción con CO_2 a alta presión. Fundamentos y aplicaciones en la industria de alimentos. *Food Science and Technology International*, 5, p.1–24.

Dixon, A.G., 1988. Correlations for wall and particle shape effects on fixed bed. *The Canadian Journal of Chemical Engineering*, 66, p.705–708.

Dixon, A.G., 1985. Thermal resistance models of packed-bed effective heat transfer parameters. *AIChE Journal*, 31, p.826–834.

Eggers, R., 1996. Supercritical fluid extraction (SFE) of oilseeds/lipids in natural products. In J. W. King & G. R. List, eds. *Supercritical Fluid Technology in Oil and Liquid Chemistry*. Champaign, IL: AOCS Press, p. 35–64.

Eggers, R. & Green, V., 1990. Pressure discharge from a pressure vessel filled with CO_2. *Journal of loss prevention in the process industry*, 3, p.59–63.

Eggers, R. & Jaeger, P.T., 2003. Extraction systems. In C. Tzia & C. Liadakis, eds. *Extraction Optimization in Food Engineering*. New York: Marcel Dekker, Inc., p. 95–136.

Gebbeken, B. & Eggers, R., 1996. Blowdown of carbon dioxide from initially supercritical conditions. *Journal of loss prevention in the process industry*, 9, p.285–293.

Gebbeken, B. & Eggers, R., 1995. Thermohydraulic phenomena during vessel release of initially supercritical carbon dioxide. *Two-phase flow modelling and experimentation*, 2, p.1139–1146.

Green, V., 1991. *Entspannung von CO_2 aus Druckbehältern unter besonderer Berücksichtigung der instationären Wärmeübertragung*. Technische Universität Hamburg-Harburg.

Green, V. & Eggers, R., 1991. Instationärer Wärmeübergang in einem Druckbehälter während des Entspannungsvorganges. *Chemie Ingenieur Technik*, 63, p.1024–1025.

Guardo, A., Coussirat, M., Recasens, F., Larrayoz, M.A. & Escaler, X., 2006. CFD study on particle-to-fluid heat transfer in fixed bed reactors: Convective heat transfer at low and high pressure. *Chemical Engineering Science*, 61, p.4341–4353.

Himmelblau, D.M. & Riggs, J.B., 2011. *Basic principles and calculations in chemical engineering* 8th Edition., Ann Arbor, Michigan: Pearson Education, Inc.

Ilyasoğlu, H., 2014. Characterization of rosehip (Rosa canina L.) seed and seed oil. *International Journal of Food Properties*, 17, p.1591–1598.

Kakaç, S., Shah, R.K. & Aung, W., 1987. *Handbook of single-phase convective heat transfer*, New York, NY: John Wiley & Sons Inc.

Kakaç, S. & Yener, Y., 1987. Basics of heat transfer. In S. Kakaç, R. K. Shah, & W. Aung, eds. *Handbook of Single-phase Convective Heat Transfer*. New York, NY: John Wiley & Sons, Inc., p. 1–35.

Kaviany, M., 1994. *Principles of convective heat transfer* F. F. Ling, ed., New York: Springer Verlag.

Laguerre, O., Amara, S. Ben & Flick, D., 2006. Heat transfer between wall and packed bed crossed by low velocity airflow. *Applied Thermal Engineering*, 26, p.1951–1960.

Lemmon, E.W., Huber, M.L. & McLinden, M.O., 2007. NIST standard reference database 23: mini-reference fluid thermodynamic and transport properties (REFPROP), version 9.0.

Liao, S.M. & Zhao, T.S., 2002a. An experimental investigation of convection heat transfer to supercritical carbon dioxide in miniature tubes. *International Journal of Heat and Mass Transfer*, 45, p.5025–5034.

Liao, S.M. & Zhao, T.S., 2002b. Measurements of heat transfer coefficients from supercritical carbon dioxide flowing in horizontal mini/micro channels. *Journal of Heat Transfer*, 124, p.413.

Long, C. & Guan, J., 2011. A method for determining valve coefficient and resistance coefficient for predicting gas flowrate. *Experimental Thermal and Fluid Science*, 35, p.1162–1168.

Mauguet, M.C., Montillet, A. & Comiti, J., 2005. Macrostructural characterization of granular activated carbon beds. *Journal of Materials Science*, 40, p.747–755.

McCabe, W.L. & Smith, J.C., 1968. *Operaciones básicas de ingenieria química*, Barcelona, Spain: Reverté S.A.

Montillet, A. & Coq, L. Le, 2001. Characteristics of fixed beds packed with anisotropic particles — Use of image analysis. *Powder Technology*, 121, p.138–148.

Núñez, G.A. & del Valle, J.M., 2014. Supercritical CO_2 oilseed extraction in multi-vessel plants. 2. Effect of number and geometry of extractors on production cost. *The Journal of Supercritical Fluids*, 92. p. 324–334.

Oosthuizen, P.H. & Carscallen, W.E., 2014. *Introduction to compressible fluid flow* 2nd Edition., Boc Raton, FL: CRC Press.

Phanikumar, M.S. & Mahajan, R.L., 2002. Non-Darcy natural convection in high porosity metal foams. *International Journal of Heat and Mass Transfer*, 45, p.3781–3793.

Pioro, I., Mokry, S. & Draper, S., 2011. Specifics of thermophysical properties and forced-convective heat transfer at critical and supercritical pressures. *Reviews in Chemical Engineering*, 27, p.191–214.

Pioro, I.L. & Duffey, R.B., 2007. *Heat Transfer and Hydraulic Resistance at Supercritical Pressures in Power-Engineering Applications*, New York, NY: ASME Press.

Pletcher, R.H., 1987. External flow forced convection. In S. Kakaç, R. K. Shah, & W. Aung, eds. *Handbook of Single-phase Convective Heat Transfer*. New York, NY: John Wiley & Sons, Inc., p. 1–67.

Reverchon, E. & Osséo, L.S., 1994. Comparison of processes for the supercritical carbon dioxide extraction of oil from soybean seeds. *Journal of the American Oil Chemists' Society*, 71, p.1007–1012.

Richter, E.A, del Valle, J.M. & Núñez, G.A, 2015. Thermodynamic properties of CO_2 during controlled decompression of supercritical extraction vessels. *Journal of Supercritical Fluids*, 98, p.102-110.

Roblee, L.H.S., Baird, R.M. & Tierney, J.W., 1958. Radial porosity variations in packed beds. *AIChE Journal*, 4, p.460–464.

Sheikholeslami, R. & Watkinson, A.P., 1998. Transient heat transfer in a fixed bed of slab-shaped and spherical particles with intraparticle conductilon. *The Canadian Journal of Chemical Engineering*, 76, p.141–147.

Smallman, R.E. & Ngan, A.H.W., 2007. *Physical metallurgy and advanced materials* 7th Edition., Oxford, UK: Butterworth-Heinemann.

Stanley, S.I., 1998. *Chemical and Engineering Thermodynamics* 3 Edition., Danvers, MA, USA: John Wiley & Sons, Inc.

Sweat, V.E., 1994. Thermal properties of foods. In M. A. Rao & S. S. H. Rizvi, eds. *Engineering properties of food*. New York: Marcel Dekker, Inc., p. 99–138.

Thadani, M.C. & Peebles, F.N., 1966. Variation of local void fraction in randomly packed beds of equal spheres. *Industrial & Engineering Chemistry Process Design and Development*, 5, p.265–268.

Wen, D. & Ding, Y., 2006. Heat transfer of gas flow through a packed bed. *Chemical Engineering Science*, 61, p.3532–3542.

Yang, K.T., 1987. Natural convection in enclosures. In S. Kakaç, R. K. Shan, & W. Aung, eds. *Handbook of Single-phase Convective Heat Transfer*. New York, NY: John Wiley & Sons, Inc., p. 1–50.

Zhang, J. et al., 2014. Depressurization study of supercritical fluid blowdown from simple vessel. *Annals of Nuclear Energy*, 66, p.94–103.

A P P E N D I X

APPENDIX 1: CALIBRATION OF THERMOCOUPLES

To check if all thermocouples were calibrated and read the same values, they were compared in a bath at homogeneous temperature before mounting the experimental device. All thermocouples were submerged to the heating bath with a temperature ranging between 57 and 58 ºC. They were connected to the MultiCon Data Logger, and data was recorded every 10 seconds. The result of the temperatures is shown in Figure A1-1 (**A**). The mean difference between each temperature measurement and the average was calculated. Then, these differences were applied as a correction factor. The effect of this correction factor is shown in Figure A1-1 (**B**). Although the variability was reduced approximately to the half or middle as the correction factors were applied, it is to be remarked that some thermocouples (*e.g.*, TR4) still presented a high variability. Therefore, the authors decided not to apply any correction factor, since temperature differences could as well come from experimental variability and not only from decalibration of the sensors. Only if necessary, a correction factor was applied to equal TR1 with TR2 if they remained different after a long equalization time.

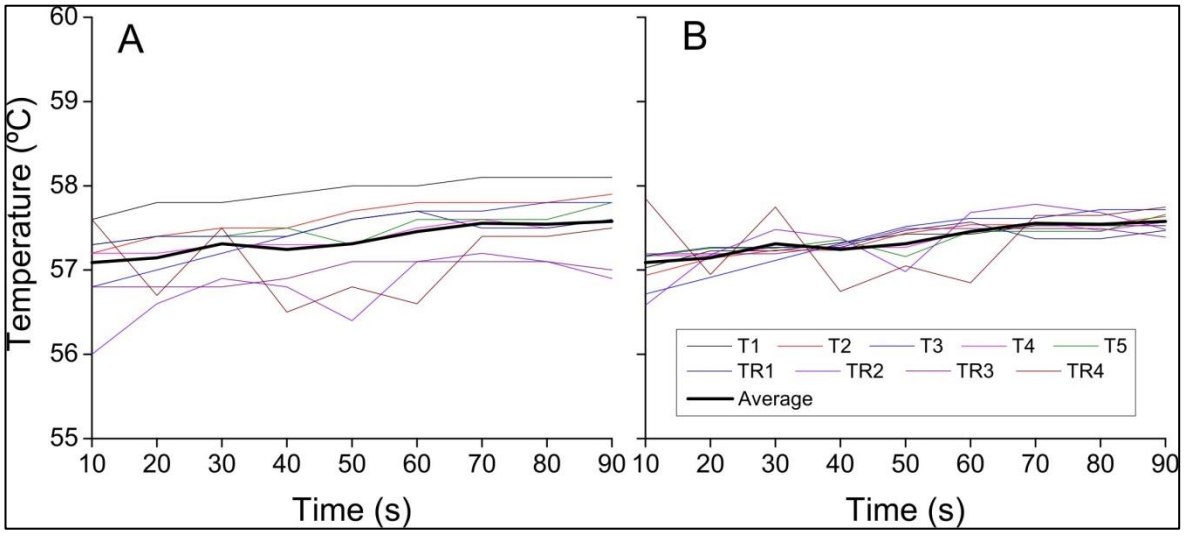

Figure A1-1. Comparison of all temperature measurements placed in a homogeneous heating bath over 90 s. (**A**) raw data; (**B**) applying a correction factor that minimizes the mean difference between each thermocouple and the average temperature.

APPENDIX 2: CALIBRATION OF VENTED FLOW MEASURING EQUIPMENT

The transient mass balance equation (Eq. 17) was integrated for the whole decompressions, to obtain the mass of CO_2 in the extractor as a function of time. Then, the integrated mass was compared to the mass in the extractor calculated as a function of the density of the CO_2 in the vessel calculated with the mean temperature of the thermocouples T1 to T4 (T5 was discarded for being the wall temperature) and the pressure in the vessel. As can be seen in Figure A2-1, the mass integrated from the mass balance was always higher than the mass calculated with internal density, whether the high-pressure vessel was charged only with CO_2 or with a packed bed as well. However, if a correction factor was applied to the mass flow rate of the vented current, the mass integrated from the mass balance fitted with the mass calculated with the internal density at the whole experiments. The higher density difference was observed near to the pseudocritical line, and was higher for experiments with a packed bed (Figure A2-1 **B**) than for experiments of empty vessels (Figure A2-1 **A**). This is because experiments with an empty vessel showed higher temperature differences than experiments with empty vessels, which leaded to uncertainty in the estimation of internal density.

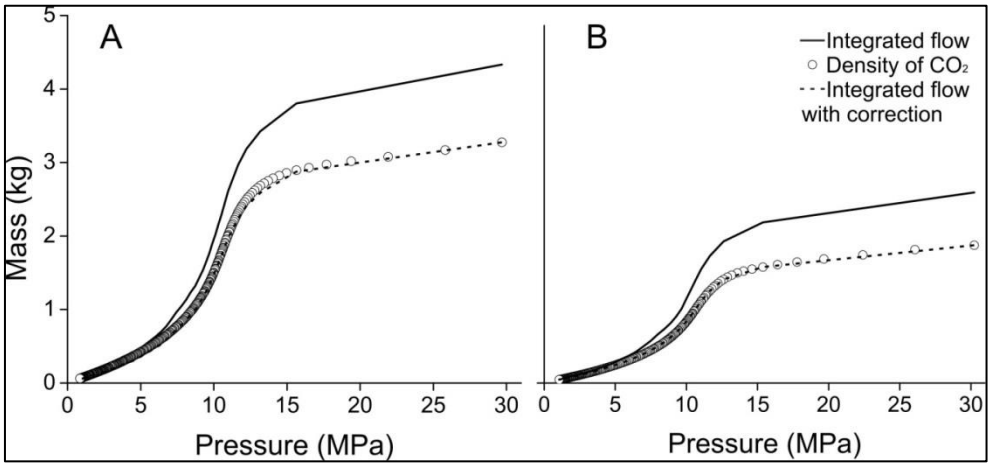

Figure A2-1. Checking of mass balance during decompressions starting at 60 ºC with a slow venting for **(A)** an empty vessel, and **(B)** a vessel packed with pressed rosehip.

APPENDIX 3: PRESSURE AND TEMPERATURES FOR DECOMPRESSIONS OF AN EMPTY VESSEL WITH DIFFERENT INITIAL TEMPERATURES AND VALVE OPENINGS

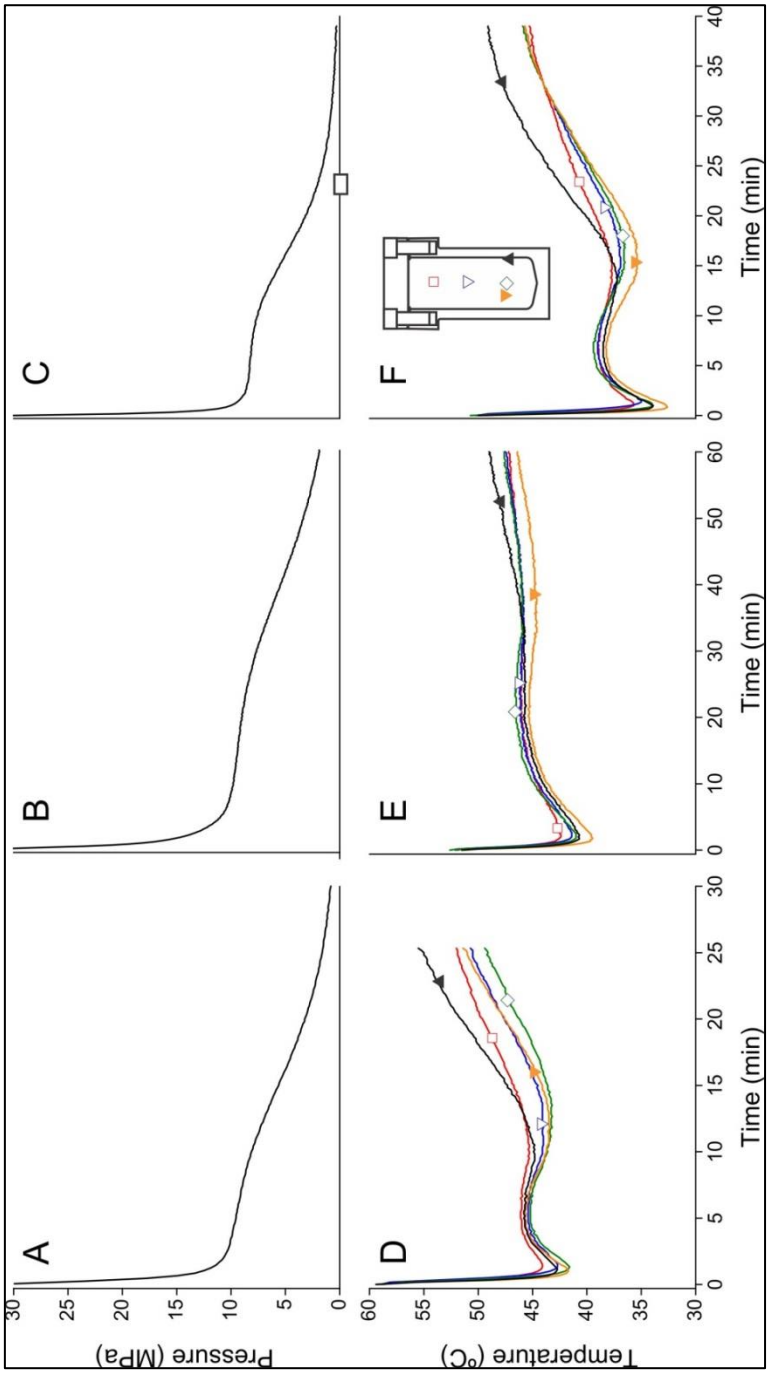

Figure A3-1. (**A**, **B**, and **C**) Pressures as a function of time for decompression of empty vessels starting at 60 ºC with a fast venting, starting at 50 ºC with a slow veniting and starting at 50 ºC with a fast venting, respectievely. (**D**, **E**, and **F**) Temperatures as a function of time for decompression of empty vessels starting at 60 ºC with a fast venting, starting at 50 ºC with a slow veniting and starting at 50 ºC with a fast venting, respectievely.

APPENDIX 4: PRESSURE AND TEMPERATURES FOR DECOMPRESSIONS OF A VESSEL CHARGED WITH DIFFERENT SUBSTRATES STRATING AT 60 ºC WITH A SLOW VALVE OPENING

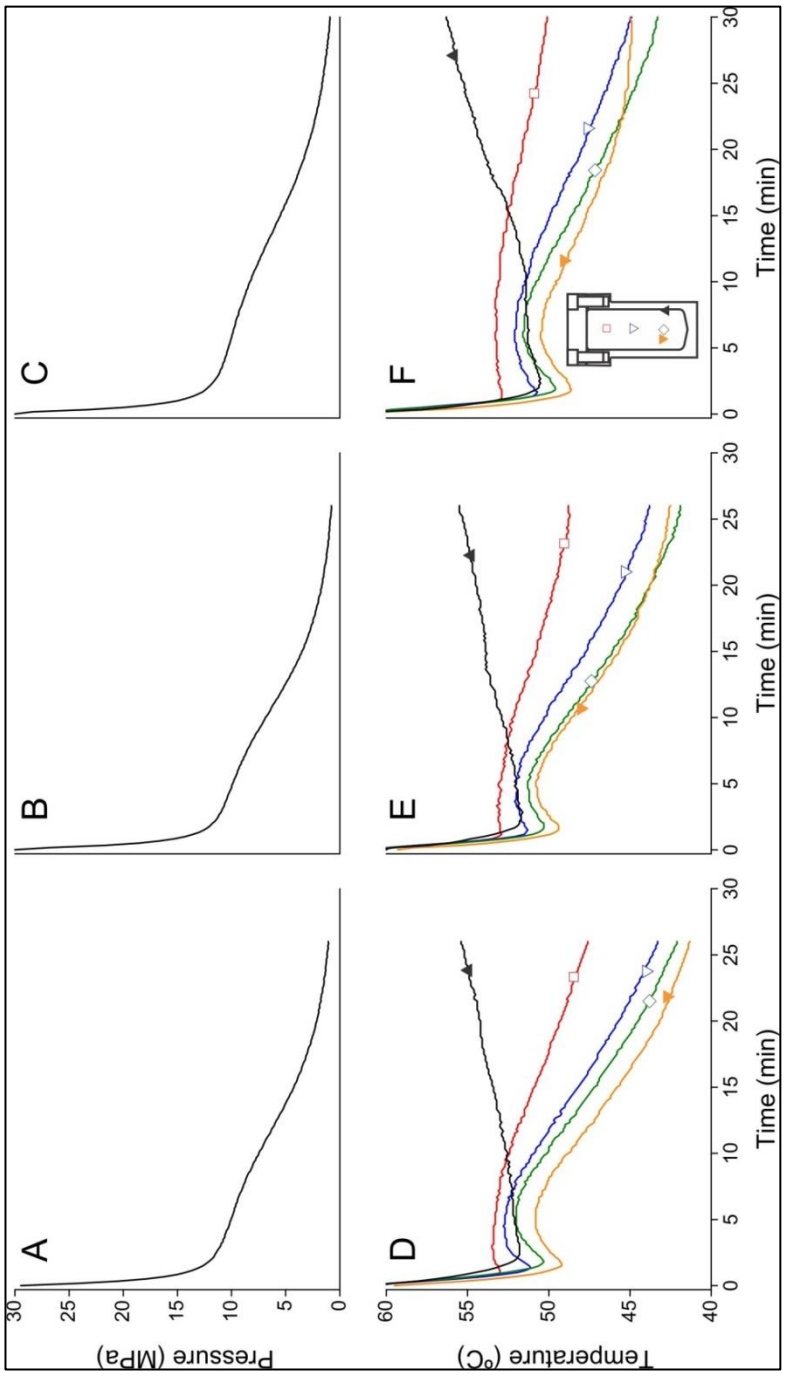

Figure A4-1. (**A**, **B**, and **C**) Pressures as a function of time for decompression of vessels packed with pelletized rosehip, pressed raspberry, and pelletized raspberry, respectievely, starting at 60 ºC with a slow venting. (**D**, **E**, and **F**) Temperatures as a function of time for decompression of vessels packed with pelletized rosehip, pressed raspberry, and pelletized raspberry, respectievely, starting at 60 ºC with a slow venting

APPENDIX 5: ENERGY BALANCE FOR A DECOMPRESSION OF AN EMPTY VESSEL

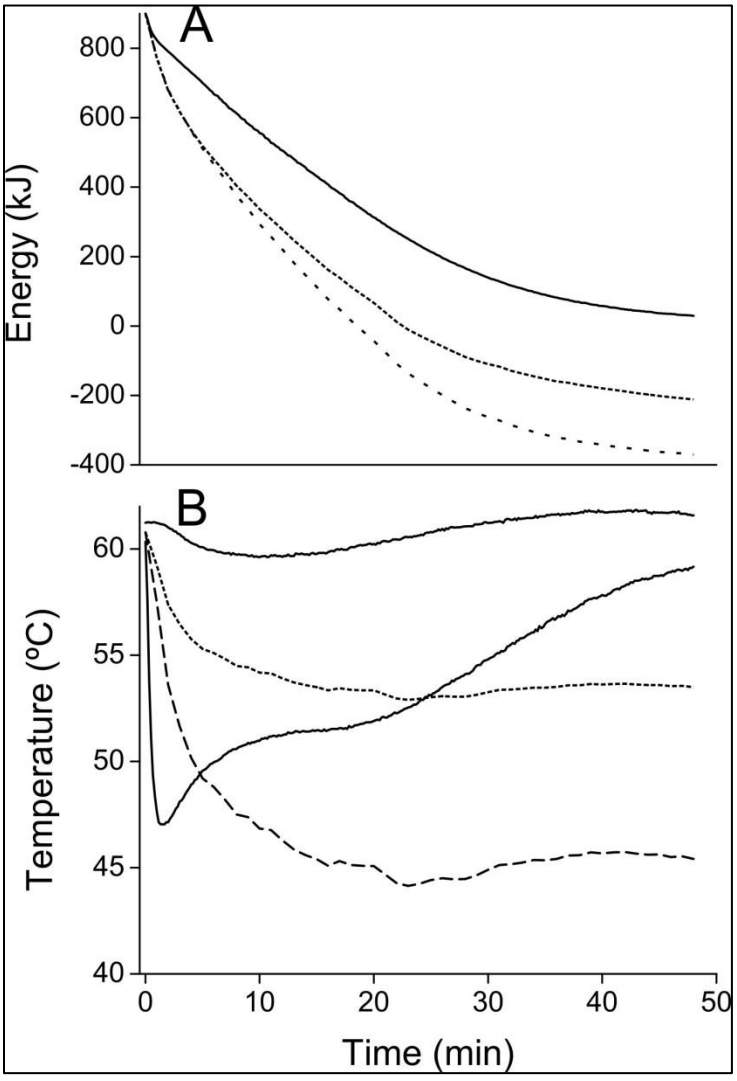

Figure A5-1. (A) Energy balance for CO_2 as a function of decompression time for slow (C_v = 0.003) decompressions starting at high temperature (60 ºC) in an empty vessel Legend: (—) Internal energy of the CO_2; and (----) Heat yield by the heating bath – enthalpy lost with the vented current; (- - -) Enthalpy lost with the vented current; (B) Estimated mean temperature of the steel of the walls of the high-pressure vessel as a function of decompression time for decompressions starting at 60 ºC in the high-pressure vessel packed with pressed rosehip. Legend: (- - -) Estimated temperature of the steel asuming that the whole vessel yields heat to the CO_2; (— - -) Estimated temperature of the steel asuming that only the walls of the vessel yields heat to the CO_2; and, (—) Inner and outer walls of the high-pressure vessel.

APPENDIX 6: REGRESSION FOR THE CORRELATIONS BETWEEN NUSSELT AND RAYLEIGH NUMBERS

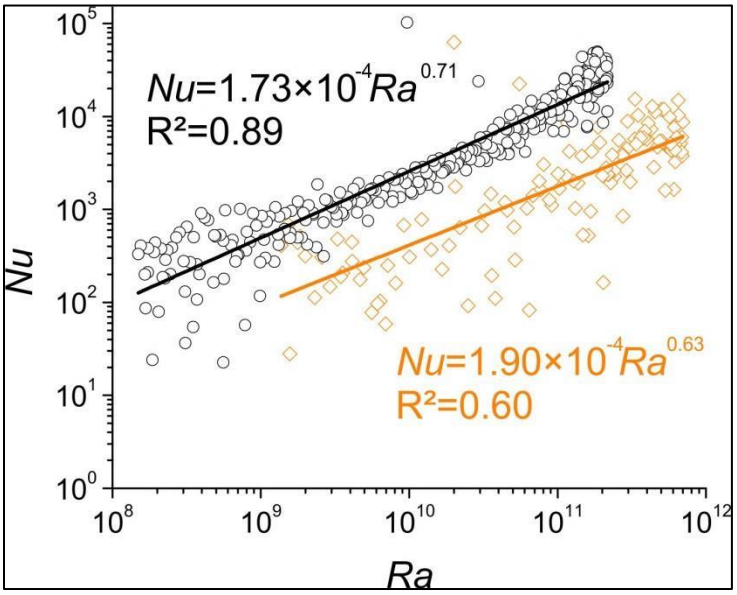

Figure A6-1. Estimation and correlation of the dimensionless Nusselt number as a function of the dimensionless Rayleigh number for an empty vessel (black) and a vessel packed with pressed rosehip (orange) during a slow decompression starting at 60 ºC.